Biomaterials Advances

Instructive electroactive electrospun silk fibroin-based biomaterials for peripheral nerve tissue engineering

--Manuscript Draft--

Manuscript Number:	MSEC-D-21-04263R2
Article Type:	Research Paper
Keywords:	Electroactive biomaterials; Electrospinning; Interpenetrating polymer network; silk fibroin; peripheral nerve regeneration
Corresponding Author:	Sarah Cartmell : The University of Manchester School of Materials MANCHESTER, UK UNITED KINGDOM
First Author:	Chinnawich Phamornnak
Order of Authors:	Chinnawich Phamornnak
	Bing Han
	Ben F. Spencer
	Mark D. Ashton
	Christopher F. Blanford
	John G. Hardy
	Jonny J. Blaker
	Sarah Cartmell
Abstract:	Aligned sub-micron fibres are an outstanding surface for orienting and promoting neurite outgrowth; therefore, attractive features to include in peripheral nerve tissue scaffolds. A new generation of peripheral nerve tissue scaffolds is under development incorporating electroactive materials and electrical regimes as instructive cues in order to facilitate full functional regeneration. Herein, electroactive fibres composed of silk fibroin (SF) and poly(3,4-ethylenedioxythiophene) polystyrene sulfonate (PEDOT:PSS) were developed as a novel peripheral nerve tissue scaffold. Mats of SF with sub-micron diameter of 190 ± 50 nm were fabricated by double layers electrospinning with thicknesses of ~100 µm (~70 – 80 µm random fibres and ~20 – 30 µm aligned fibres). Electrospun SF mats were modified with interpenetrating polymer networks (IPN) of PEDOT:PSS in various ratios of PSS/EDOT (α) and the polymerization was assessed by hard X-ray photoelectron spectroscopy (HAXPES). The mechanical properties of electrospun SF and IPNs mats were characterized by the wet state tensile and the electrical properties were examined by cyclic voltammetry (CV) and electrochemical impedance spectroscopy (EIS). The cytotoxicity and biocompatibility of the optimal IPNs (α = 2.3 and 3.3) mats were ascertained via the growth and neurite extension of mouse neuroblastoma x rat glioma hybrid cells (NG108-15) for 7 days. The longest neurite outgrowth of 300 µm was observed in the parallel direction of fibre alignment on laminin-coated electrospun SF and IPN (α = 2.3) mats which is the material with the lowest electron transfer resistance (R_{et}, ca. 330 Ω). These electrically conductive composites with aligned sub-micron fibres exhibit promise for axon guidance and also has the potential to be combined with electrical stimulation treatment as a further step for the effective regeneration of nerves.
Suggested Reviewers:	Sheila Mcneil The University of Sheffield s.macneil@sheffield.ac.uk
	Brian Cousins Loughborough University B.Cousins@lboro.ac.uk
	Anita Ghag University of Birmingham a.k.ghag@bham.ac.uk

Response to Reviewers:	

Editor and Reviewer comments:

Reviewer #1:

The authors answered some of my questions.

However, regarding conductivity of the scaffold, the authors answered that it has already been measured on similar fibers made by their group. I do not think the two types of fibers are similar, and certainly the conductivity is not the same. Indeed, in the previous article cited the PEDOT-PSS was deposited after electrospinning on the surface of the fibers, and further treated with DMSO to increase its conductivity. In the case of this paper, the authors have polymerized the EDOT directly into the nanofibers to form a fibroin/PEDOT-PSS IPN. In this case PEDOT-PSS should be in the bulk of the fibers and not only on the surface. Moreover, we do not know if the amount is large enough to ensure continuity of the PEDOT/PSS along the nanofibers. Only the measurement of the conductivity can prove that it is the case.

Moreover, the cited article is not described in the introduction of this article, and comparison and discussion of the two different approaches should be done: coating of the fibers with PEDOT/PSS vs IPN.

Response: Thank you for your constructive criticism. We agree that the SF/PEDOT:PSS fibre fabricated via IPN is different from a previous study by our group. We do not want to compare which approach (IPN vs. coating) is better since almost all manufacturing protocols are different (e.g. silk preparation, electrospinning parameters, PEDOT:PSS concentration). In this study, we would like to present that as well as a coating method, IPN is another successful approach to modifying electrospun SF, which is an electrical insulator, to be an electrically conductive material.

To clarify the conductivity of IPN materials,

(1) we define the conductivity of electrical insulators, semiconductors, and conductors in the introduction, in lines 63 – 66.

(2) we measure the conductivity of SF and IPNs fibres using two-point probe system as explain in the materials and methods, in lines 187 – 199.

The results were shown in lines 356 – 357 and supplementary information, table S2.

(3) we discuss the conductivity of IPN materials (this work) in comparison with the conductivity of coating materials (previous work of our group), as shown in lines 491 – 496. This result shows that SF/PEDOT:PSS is semiconductor.

Highlights

- Electrospinning SF solution produces non-woven mats via a dialysis free method, rendered stable by solvent treatment.
- SF fibre alignment is possible via electrospinning produces instructive mats which encourage neurite extension aligned with the fibres.
- IPN effectively modifies electrospun SF non-woven mats yielding electroactive non-woven mats.
- IPN mat ($\alpha = 2.3$) coating with laminin promotes the longest neurite extension following the alignment of fibres.

Declaration of interests

☒ The authors declare that they have no known competing financial interests or personal relationships that could have appeared to influence the work reported in this paper.

☐The authors declare the following financial interests/personal relationships which may be considered as potential competing interests:

Chinnawich Phamornnak: Methodology, Formal analysis, Writing – Original Draft, Writing – Review & Editing **Bing Han:** Methodology **Ben F. Spencer:** Formal analysis, Writing – Original Draft **Mark D. Ashton:** Methodology, Writing – Original Draft **Christopher F. Blanford:** Investigation, Resource **John G. Hardy:** Formal analysis, Writing Review & Editing, Supervision **Jonny J. Blaker:** Conceptualization, Supervision, Project administration **Sarah H Cartmell:** Conceptualization, Supervision, Project administration, Funding acquisition

Instructive electroactive electrospun silk fibroin-based biomaterials for peripheral nerve tissue engineering

Chinnawich Phamornnak[a], Bing Han[a], Ben F. Spencer[a], Mark D. Ashton[d], Christopher F. Blanford[a,b,c], John G. Hardy[d,e], Jonny J. Blaker[a,f,*] Sarah H. Cartmell[a,*]

[a]Department of Materials and Henry Royce Institute, University of Manchester, Manchester, United Kingdom

[b]Manchester Institute of Biotechnology, University of Manchester, Manchester, United Kingdom

[c]National Graphene Institute, University of Manchester, Manchester, United Kingdom

[d]Department of Chemistry, Lancaster University, Lancaster, United Kingdom

[e]Materials Science Institute, Lancaster University, Lancaster, United Kingdom

[f]Department of Biomaterials, Institute of Clinical Dentistry, University of Oslo, Oslo, Norway

*Corresponding authors at: Department of Materials, University of Manchester, Sackville Street Building, Manchester, M1 3BB, United Kingdom. Tel: +44 (0) 161 306 3567. Email address: jonny.blaker@manchester.ac.uk and sarah.cartmell@manchester.ac.uk

Abstract

Aligned sub-micron fibres are an outstanding surface for orienting and promoting neurite outgrowth; therefore, attractive features to include in peripheral nerve tissue scaffolds. A new generation of peripheral nerve tissue scaffolds is under development incorporating electroactive materials and electrical regimes as instructive cues in order to facilitate full functional regeneration. Herein, electroactive fibres composed of silk fibroin (SF) and poly(3,4-ethylenedioxythiophene):polystyrene sulfonate (PEDOT:PSS) were developed as a novel

peripheral nerve tissue scaffold. Mats of SF with sub-micron diameter of 190 ± 50 nm were fabricated by double layers electrospinning with thicknesses of ~100 µm (~70 – 80 µm random fibres and ~20 – 30 µm aligned fibres). Electrospun SF mats were modified with interpenetrating polymer networks (IPN) of PEDOT:PSS in various ratios of PSS/EDOT (α) and the polymerization was assessed by hard X-ray photoelectron spectroscopy (HAXPES). The mechanical properties of electrospun SF and IPNs mats were characterized by the wet state tensile and the electrical properties were examined by cyclic voltammetry (CV) and electrochemical impedance spectroscopy (EIS). The cytotoxicity and biocompatibility of the optimal IPNs (α = 2.3 and 3.3) mats were ascertained via the growth and neurite extension of mouse neuroblastoma x rat glioma hybrid cells (NG108-15) for 7 days. The longest neurite outgrowth of 300 µm was observed in the parallel direction of fibre alignment on laminin-coated electrospun SF and IPN (α = 2.3) mats which is the material with the lowest electron transfer resistance (R_{et}, ca. 330 Ω). These electrically conductive composites with aligned sub-micron fibres exhibit promise for axon guidance and also has the potential to be combined with electrical stimulation treatment as a further step for the effective regeneration of nerves.

Keywords: Electroactive biomaterials, Electrospinning, Interpenetrating polymer network, Silk fibroin, Peripheral nerve regeneration

1. Introduction

Peripheral nerve injury (PNI) is a severe problem for trauma patients worldwide [1]. Although injured nerves can regenerate themselves, the level of functional recovery is often unsatisfactory and it is very challenging to delivery full recovery due to the limitations of neural sizes, distances, regeneration periods, etc. [2]. The most recent research trends have focused on "active" environments for regeneration such as the use of stem cells [3-6], external electrical stimulation [7-10], and electrically conductive scaffolds [11-15] in order to accelerate regenerative outcomes. One of the promising materials for developing tissue scaffolds is silk fibroin (SF) from *Bombyx mori* silk cocoons.

SF fibres are natural biocompatible materials with high mechanical strength, which can be dissolved and processed into many forms (such as films, foams, hydrogels, and fibres) [16-18]. SF is predominantly composed of heavy (H) and light (L) chain fibroins connected via disulfide bonds and glycoprotein P25. The H-chain is a repeating amino acid sequence of glycine – alanine – glycine – alanine – x, where x is serine or tyrosine [19]. The fibres have a high content of antiparallel β-sheets, hydrophobic and crystalline structures, which play a key role in the strength of the fibres, and the L-chain is a smaller hydrophilic structure [20, 21]. The electrospinning of SF has been studied for its potential application in peripheral nerve regeneration for a decade, showing promising results for neural growth and neurite extension, *in vitro* [12, 22, 23]. While electrospinning silk is time-consuming and environmentally dependent (particularly on the humidity of the spinning chamber), it produces materials with biomimetic structures. Das et al., 2017 showed that electrically conductive SF scaffolds promoted stronger action potentials at the distal end of the injured site compared to non-conductive SF scaffolds *in vivo* [12], suggesting the

electroactive SF may promote full functional nerve regeneration, and motivating the development of variants of conductive SF scaffolds for tissue engineering.

Electrical conductors, semiconductors, and insulators are defined by their conductivity. Typically conductors have conductivities from $10^4 – 10^7$ S/m (e.g., metals), semiconductors from $10^{-6} – 10^4$ S/m, and insulators from $10^{-20} – 10^{-10}$ S/m [24-26]. Logically, SF has been reported as an electrical insulator with the conductivity range of $10^{-17} – 10^{-11}$ S/m [27-29]. Various conductive materials including polypyrrole (PPy) [23, 30, 31], polyaniline (PANi) [12], graphene oxide (GO) [23], reduced graphene oxide (rGO) [23, 32], poly(3,4-ethylenedioxythiophene) (PEDOT) [22], and PEDOT doped with polystyrene sulfonate (PEDOT:PSS) [33, 34] have been combined with electrospun SF. These conductive materials can stably blend with SF-based materials due to the physical and non-covalent crosslinks (including hydrogen bonding and electrostatic interactions) within SF-based materials [33]. In this study, PEDOT:PSS was chosen for SF modification due to its low cost, high conductivity, high thermal stability and water solubility (facilitating processing, storage and sterilization) [35, 36], and moreover, for peripheral nerve tissue engineering applications it can support cell proliferation and promote the expression of neurogenic differentiation factors such as MAP2 and β-III tubulin [37, 38]. Furthermore, electrical stimulation through the PEDOT:PSS incorporated scaffold affects the cell alignment and enhances the length of neurite extension [37].

Even though rat adrenal pheochromocytoma cell line (PC-12) is commonly used in neural regeneration, particularly neurite outgrowth [13, 31, 32, 39-41], mouse neuroblastoma x rat glioma hybrid cell (NG108-15) is preferred in this study due to the electrophysiology. Typically, NG108-15 is used in the study of action potential of nerves [42-46]; however, many previous studies also

used NG108-15 for neuron regeneration [47-51]. Therefore, NG108-15 can use for both the neurite extension study and the functionality of the regrowth nerve via the electrophysiology. It is to be hoped that NG108-15 will be an attractive cell line for peripheral nerve regeneration, especially to study the action potential of cells grown on electrically conductive material with electrical stimulation in the future.

This study aims to develop the electrically conductive tissue scaffolds based on electrospun SF for peripheral nerve regeneration. The strategy of double layer electrospinning is designed for material reinforcement and enhancing the properties of the processed materials. The thick layer of random fibres is the base layer with a thinner layer of aligned fibres on top to instruct the direction of neurite outgrowth [11]. The novel protocol for electrospinning such mats was optimised to reduce the time-consumed by dialysis. The electrical properties of the electrospun SF mats were modified via growth of an interpenetrating polymer network (IPN) of PEDOT:PSS. The IPN mats were cultured with a neural-like cell line (NG108-15) in order to study the neural growth and neurite extension profiles on the materials. The knowledge generated by this study presents another step towards the development of a conductive scaffold leading to the successful functional recovery of peripheral nerve injuries, with the potential to apply electrical stimulation in future studies.

2. Materials and methods

2.1 SF preparation

Bombyx mori silk cocoons were cut into small pieces and 5 g was then boiled at 80°C in 2 L of 0.02 M sodium carbonate (Na_2CO_3, Sigma-Aldrich) for 30 min with gentle stirring to disperse the silk fibres. The degummed SF was washed 3 times by stirring in distilled water for 20 min followed by replacing the water. The purified SF was squeezed well, stretched on a tray, and left overnight in a fume cupboard for the water to evaporate.

A solution of 10% wt/v degummed SF in non-aqueous medium was used for electrospinning. A solution of formic acid (FA, 98-100%, Fisher) and calcium chloride ($CaCl_2$, fused, granular, Fisher) with the ratio of 98 mL FA to 2 g $CaCl_2$ was prepared. The FA-$CaCl_2$ solution was used for the dissolution of SF (1 g of SF in 10 mL of FA-$CaCl_2$) by shaking with a vortex for a few minutes until the SF was completely dispersed in the solution, after which the SF solution was incubated at 45°C in a water bath overnight, and the solution turned dark pink in colour. The solution was filtered to get rid of debris that may block the electrospinning needle using a vacuum pump and a borosilicate glass filter (Pyrex®, porosity grade 1) prior to electrospinning.

2.2 Double layers electrospinning SF

The electrospinning solution (SF in FA/$CaCl_2$) was transferred to a 10 mL plastic syringe (BD Plastipak) with a flattened 19 G needle (BD Plastipak). It was then placed in a vertical electrospinning setup within an environmentally controlled chamber to fabricate the base layer of randomly aligned fibres. The tip of needle was placed 12 cm above the edge of the rotating mandrel with a width and diameter of 5 cm and 12 cm, respectively. Greaseproof paper (5 x 38 cm^2) was used as a collector and was wrapped around the width of the mandrel. The syringe was operated

at 0.4 mL/h constantly for 8 h by a syringe pump (Cole-Parmer). Meanwhile, the high voltage of 35 kV generated by DC voltage supplies was applied to the system (+30 kV at the needle and -5 kV at the rotating mandrel). The rotating speed of the collector was 800 rpm (5.03 m/s linear speed). Relative humidity (R.H.) and temperature were controlled at 35% R.H. and 25°C all the time.

After that, the collector and the SF solution in a syringe were relocated and placed in a horizontal electrospinning setup with the high rotating speed collector in order to deposit a layer of aligned fibres on top of the base layer of randomly aligned fibres. The working distance and feed rate were 12 cm and 0.4 mL/h; however, the voltage supply was reduced to 15 kV (+15 kV at the needle and 0 kV at the collector) and the rotating speed of collector was increased to 1500 rpm (9.42 m/s linear speed), and run for 4 h, yielding electrospun bilayer mats with thicknesses of ca. 100 μm. The thickness of fibre mat was measured by using a micrometer (DML3032, Digital Micrometers Ltd). Finally, electrospun SF mats were immersed in 80% ethanol for 20 min to induce β-sheet formation.

2.3 IPN of PEDOT:PSS on electrospun SF

3,4-ethylenedioxythiophene (EDOT, Sigma-Aldrich) was dispersed at 0.5% w/v in an aqueous solution of initiators containing 0.98% w/v sodium persulfate ($Na_2S_2O_8$, Sigma-Aldrich), and 0.2% w/v iron (II) sulfate heptahydrate ($Fe_2SO_4 \cdot 7H_2O$, Sigma-Aldrich) [52]. The dopant polystyrene sulfonate (PSS, Sigma-Aldrich) was added to the EDOT dispersion with various molar ratios to EDOT monomer (α) from 1.3 to 3.3 (approximately 0.84 – 2.13% wt/v) to produce a homogenous solution. The post-treated electrospun SF mats were immediately immersed in the working solution and left for 72 h at room temperature for polymerization and IPN formation. Over the

course of the reaction the solution changed from yellow to dark blue. After 72 h, the dark blue IPN materials were washed twice and preserved in distilled water to avoid shrinkage.

2.4 FTIR and HAXPES

The secondary structure of the SF was characterized by attenuated total reflectance – Fourier transform infrared spectroscopy (ATR – FTIR). The FTIR spectra were recorded between 4000 – 400 cm^{-1}. The amide I band (1700 – 1600 cm^{-1}) was analysed and deconvoluted using Origin software (OriginLab, USA). Three main structures; β-sheet, random coil, turns and bends were observed, assigned according to Wilson et al., 2000 [53]. β-sheets were assigned between 1621 – 1629 cm^{-1} and 1671 – 1679 cm^{-1}, random coils between 1641 – 1649 cm^{-1}, turns and bends were assigned between 1658 – 1671 cm^{-1} and 1681 – 1696 cm^{-1}, respectively.

The quantity of sulfur (S) present in PEDOT:PSS was determined by hard X-ray photoelectron spectroscopy (HAXPES-lab, Scienta Omicron GmbH), which uses a Ga Kα X-ray source (9.25 keV, Excillum), where an increase in kinetic energy of the emitted photoelectrons leads to an increase in sampling depth compared to surface-sensitive XPS using X-rays at energies of 1-2 keV [54, 55]. This allows for the bulk-like composition to be measured, minimizing the influence of surface contamination. Samples were attached to Omicron sample plates using adhesive copper tape for measurements under ultra-high vacuum with a base pressure of 6×10^{-10} mbar. A charge neutralizing low energy electron gun (FS40A, PREVAC) was used to replenish the electron supply after photoexcitation. The EW4000 electron energy analyzer with an entrance slit width of 1.5 mm was used to measure survey spectra, using a pass energy of 500 eV with an energy resolution of ~2 eV, and core level spectra of the elements of interest (C 1s at 285 eV binding energy (BE), N 1s at 400 eV BE, O 1s at 530 eV BE, and S 1s at 2470 eV BE), measured with 200 eV pass energy

with an energy resolution of ~0.8 eV [56]. Atomic concentrations were obtained using calculated sensitivity factors for the core levels, as described in [57] using recently published photoionization parameters up to 10 keV [58, 59]. The sampling depth, defined as $3\lambda \cos\theta$, where λ is the inelastic mean free path of electrons and θ is the electron take-off angle with respect to the surface normal [60], was calculated to be ~54 nm using the TPP-2M formula [61]. By tilting the sample and increasing the electron take-off angle, the sampling depth can be reduced towards the surface; θ was varied up to 70° to reduce the sampling depth to ~18 nm, and with combined Al Kα (1486 eV) XPS reduced the sampling depth to ~11 nm. Data were analyzed using CasaXPS [62].

2.5 Electrochemical characterisation

Cyclic voltammetry (CV) measurements were performed using a PalmSens EmStat 3+ potentiostat connected to a personal computer using the PSTrace 7.4 software, whereas electrochemical impedance spectroscopy (EIS) measurements were performed using an Ivium-n-Stat Multichannel Electrochemical Analyzer. For CV and EIS measurements, a three-electrode system was used with an Ag/AgCl reference electrode (CH Instruments, Inc. Austin, TX, USA), a platinum wire counter electrode (Sigma Aldrich, Gillingham, UK), and a working electrode (electrospun SF and IPN mats were cut into rectangular pieces of 1 x 3 cm, attached to glass slide by carbon tape prior to use). The electrodes were in a buffer (4 mL of phosphate-buffered saline [PBS] at pH 7.4) that was degassed with N_2. For CV measurements, the potential was swept between −1.0 V and +1.0 V vs. the Ag/AgCl electrode at a scan rate of 0.05 Vs^{-1}. For EIS measurements, the PBS also contained 5 mM of $[Fe(CN_6)]^{3-/4-}$, and measurements were performed with an open-circuit potential of 230 mV, with an amplitude of applied potential perturbation of 10 mV in the frequency range of 0.1 – 105,000 Hz.

2.6 Electrical conductivity

The conductance of fibres were measured in accordance with protocol IPC-TM-650, number 2.5.17.2 described by the Institute for Interconnecting and Packaging Electronic Circuits. Fibres supported on glass slides were examined by chronoamperometry using a Keithley 2612B source meter (Tektronix, Beaverton, US). Chronoamperometric measurements were made with a two-point probe system (copper alligator clips), by connecting counter and reference electrodes together. Briefly, two thin strips of adhesive-backed copper tape (Ted Pella, Inc., Redding, CA) were attached to the films, parallel to one another, separated by a distance of 0.5 cm. The working and counter electrodes were clipped on the strips of copper tape, and the current measured for 30 seconds during a potential step experiment at 10 V. The electrodes were moved to different positions after each measurement, and the current passed was recorded at three different positions. The conductivity (S/m) of the fibre was determined in accordance with equations (Supplementary information, table S2).

2.7 Tensile tests

The ultimate tensile stress (MPa), strain at break, Young's modulus (MPa), and toughness (kJ/m^3) were tested by wet-state, horizontal tensile under water (ElectroForce, Planar Biaxial, TA Instruments). Electrospun SF and IPNs mats were cut into small rectangular pieces of 5 x 35 mm^2, with the direction of fibre alignment parallel to the sample length. The thicknesses of samples were measured by a micrometer (DML3032, Digital Micrometers Ltd). The initial length between tensile grips was 25 mm (5 mm of both ends were clamped). One grip connected to a load cell of 22 N was dynamic end with the moving speed of 10 μm/s, while another grip was stationary end.

2.8 NG108-15 cell culture

NG108-15, mouse neuroblastoma x rat glioma hybrid cells, were cultured in Dulbecco's Modified Eagle Medium (DMEM, Sigma) with high glucose supplemented with 10% fetal bovine serum (FBS), 1X – HAT solution (Fisher), and 1% antibiotic as a growth medium. They were incubated at 37°C, 5% CO_2. The medium was refreshed every 2 days until the cell confluence reached 60 – 70%, it was changed to a differentiation medium, growth medium with 0.75 mM cyclic adenosine monophosphate (cAMP, Stratech).

2.9 Media-extracting assay

The cytotoxicity of the electrospun SF and IPNs materials were tested by extracting assay (conditioned medium). The materials were cut into pieces of 3 x 3 cm^2, and sterilized with 70% ethanol for 10 min and UV exposure for 15 min. The materials were incubated with 6 mL of the growth medium at 37°C for 24 h. The extracted medium was exposed to NG108-15 in the subconfluent state. The cell morphology was observed, a live/dead assay undertaken, and DNA concentration determined for 72 h after exposure.

2.10 In Silico Toxicity Screening

In silico toxicity screening was carried out using Derek Nexus (v. 6.0.1, Nexus: 2.2.2) and Sarah Nexus (Sarah Nexus: 3.0.0, Sarah Model: 2.0) supplied by Lhasa Limited, Leeds, UK. Simplified molecular-input line-entry system (SMILES) notations for species analyzed are: formic acid, [H]C(O)=O; sodium persulfate, S(OOS([O-])(=O)=O)(=O)(=O)[O-].[Na+].[Na+]; EDOT, C1=C2C(=CS1)OCCO2; PEDOT, O1CCOC=2C1=C(SC=2C)C; PSS, C1=CC(=CC=C1C(CC)C)S(=O)(=O)[O-].

2.11 Direct contact assay

NG108-15 were cultured directly on electrospun SF and IPNs substrates. These materials were cut and mounted on 12 x 12 cm^2 glass coverslips. Materials were sterilized with 70% ethanol for 10 min and UV exposure for 15 min. They were washed twice with Dulbecco's phosphate buffer saline (DPBS, Sigma) and then incubated with 5 µg/mL laminin at 37°C for 2 h. NG108-15 cultured in a T-75 flask were trypsinized and placed on sample with the seeding density of 5 x 10^3 cells/cm^2 and cultured for 7 days. The growth medium was refreshed every 2 days. For the neurite extension study, the growth medium was changed to the differentiation medium at day 2, and continuously refreshed every 2 days. The cell metabolic activity, DNA concentration, and neurite length extension were observed for 7 days.

2.12 Cell metabolic activity and DNA concentration assays

Metabolic activity and DNA concentration were performed via resazurin and dsDNA PicoGreen® assays. They were determined at day 1, 3, 5, and 7. Samples with NG108-15 were washed twice with DPBS followed by 1 h incubation at 37^o C with growth medium containing 12.5 µg/mL of resazurin sodium salt (Sigma-Aldrich). Next, 100 µL medium was collected and the fluorescence intensity was measured.

Either NG108-15 cells or fibres with NG108-15 cells were taken from glass coverslips and put in 1.5 mL microcentrifuge tubes. 500 µL 1X Tris-EDTA (TE) buffer were added into the tubes, repeated freeze-thaw process three times, and centrifuged. 100 µL supernatants were collected and mixed with 100 µL PicoGreen® working solution for measuring fluorescence intensity. The excitation/emission of 544/590 nm and 485/520 nm with a Microplate Reader (FLUOstar) were used for resazurin and PicoGreen® assays respectively.

2.13 Live/dead assay

Live/dead assay is only used to determine the toxicity of chemical residues from fibre mats in the media-extracting assay (conditioned medium). Qualitative analysis of cell viability was observed by fluorescent microscopy (Nikon Eclipse 50i) with 10X magnification. Calcein AM (Invitrogen) and ethidium homodimer (EthD-1, Invitrogen) were diluted in DPBS, their final concentrations were 2 µM and 4 µM, respectively. Cells were stained with this working solution for 10 min at 37°C. Live cells were observed as uniform green in cytoplasm, while dead cells were shown as bright red spots at nucleus. The excitation/emission 495/515 nm and 495/635 nm were used for live and dead cells, respectively.

2.14 Scanning electron microscopy (SEM)

Typically, the surface of electrospun SF, IPNs mats, and also the neurite length of NG108-15 on substrates were observed by SEM (TESCAN MIRA3 and TESCAN VEGA3). Samples of NG108-15 were fixed with 2.5% glutaraldehyde in PBS for 30 min at 4°C and washed twice with PBS. After that, they were sequentially dehydrated through the series of ethanol gradients; 50%, 70%, 90%, and 100% for 5 min/each. Lastly, hexamethydisilazane (HDMS) was added to samples and they were left in a fume cupboard for evaporation of the HMDS overnight. The dried samples were then prepared and sputtered with Au/Pd (5 nm thickness) using an automatic gold sputter coater (Quorum) followed by SEM observation.

The direction of aligned fibres was always rotated to the position of 90º (12 o'clock) following the Cartesian coordinating system. The images were saved and collected in the format of .tif file. The fibre diameter, neurite length, and neurite orientation were then analysed using ImageJ software. The polarscatter and polarhistogram of neurite lengths were plotted using Matlab software

(MATLAB R2020a). Additionally, the oval profile plugin was used for measurement of fibre alignment and the 2D FFT alignment was calculated following it was mentioned in Ayres et al., 2008 [63]. The angle positions of 0° – 180° were considered in this study.

2.15 Immunofluorescence staining

β-III tubulin, an element of microtubule commonly found in neurites, was stained and qualitatively observed with a confocal microscope (CQ1, Yokogawa). Samples were fixed with 4% paraformaldehyde for 15 min. They were washed twice with PBS and permeabilised by adding 500 µL of Q & P solution (0.5% Triton X-100 in 0.2 M glycine in PBS) on each sample for 5 min at room temperature. After that, samples were washed twice with PBS and blocked non-specific proteins by adding 300 µL 2% fish skin gelatin (FSG) for 30 min. The primary antibody, rabbit polyclonal to β-III tubulin, were diluted in 2% FSG and incubated with the sample at 4°C overnight. The sample were washed twice again prior to the secondary antibody staining. Goat anti-rabbit IgG H&L (Alexa Fluor® 488) and DAPI were diluted in 2% FSG, added onto samples, and then incubated for 2 h in the dark area. The stained samples should be washed twice again, mounted onto glass slides with a prolonged mounting agent.

2.16 Statistical analysis

Data collected from samples were analysed by GraphPad Prism 8 software. Electrospun SF without PEDOT:PSS was used as a control parameter. Two-way ANOVA (Tukey) with $p < 0.03$ were considered as statistically significant.

3. Results

3.1 Preparation of electrospun SF

Double layers electrospun SF mats have the thickness of ~100 μm after 12 h electrospinning. The average diameters of fibres of the top (aligned fibre) and base (randomly aligned fibre) layers were relatively similar, 188 ± 55 nm and 177 ± 48 nm respectively. Ethanol-treatment and PEDOT:PSS IPN formation have no statistically significant effect on the fibre diameters (Supplementary information, Figure S1). The distributions of fibre diameters are shown in Figure 1c. The 2D FFT alignment results show the significant difference between the top and base layers. The peak of 2D FFT alignment value of the top layer was 2.25 at the positions of 88° – 90°, while that of the bottom layer was 9 times lower, it was 0.25 at the positions of 82° – 91° as shown in Figure 1d.

The secondary structure of the silk-based materials are altered by ethanol treatment, as confirmed by the FTIR results shown in Figures 1e and 1f. The amide I peak of electrospun SF was shifted from the wavenumber of 1651 cm^{-1} to between 1625 and 1621 cm^{-1} (indicative of β-sheet formation). The deconvolution of the amide I band spectra also reveals that the total secondary protein structures of untreated electrospun SF contains 55% β-sheet. Almost all ethanol treatment conditions increased β-sheet formation up to 63 – 65% except the condition of 70% ethanol.

Bulk – sensitive HAXPES demonstrates that the IPN formation protocol is a more effective method to generate electroactive SF-based biomaterials than dip coating (Supplementary information, Figure S2). Both surface – sensitive XPS and bulk – sensitive HAXPES show that the relative percentage of Sulfur (%S) to all elements (C, O, N, and S) of IPNs mats are higher than that of electrospun SF as shown in Figure 2. The relative %S of IPNs mats at the surface (~11 nm) were significantly higher than the other depths (~19 – 54 nm). It was 3.1% at the surface and

decreased to 1.6% over bulk material for IPN (α = 2.3), while it was 2.8% at the surface and decreased to 1.3% over bulk material for IPN (α = 3.3). Moreover, the fitting of the peaks of S 2p and S 1s of XPS and HAXPES confirm the successful polymerisation of PEDOT:PSS on/in electrospun SF as shown in Figure 2c. Each S 2p chemical species was fit with a spin-orbit split doublet, whereas the S 1s singlet state requires one peak for each chemical species. The spectra show two chemical species associated with PEDOT (S 2p3/2 at ~164 eV, S 1s at ~2472 eV binding energy) and PSS (S 2p3/2 at ~168 eV, S 1s at ~2477 eV binding energy) [64-66]. The relative amount of PSS and PEDOT is quite similar at both sampling depths for IPN (α = 2.3). It was 73% PSS at 11 nm, 69% at 54 nm for IPN (α = 2.3) and it was 78% PSS at 11 nm, 62% at 54 nm for IPN (α = 3.3).

The chemical states of C, N, O and S were also measured using XPS and angle-resolved HAXPES (Supplementary information, Figures S3 – S6). These results show little change in the relative amounts of each chemical state (e.g. the amount of PSS and PEDOT) from the surface into the bulk, suggesting a good level of polymerization has been achieved and that the simple IPN formation protocol yields a homogenous material (similar to reports of IPN generation in silk fibroin films [67], but in contrast to reports of IPN generation using silk fibroin materials that required two rounds of IPN formation to yield homogenous IPNs [11, 30]). The C 1s spectra indicate some excess hydrocarbon at the surface, and the N 1s spectra suggest some protonation at the surface, as is expected.

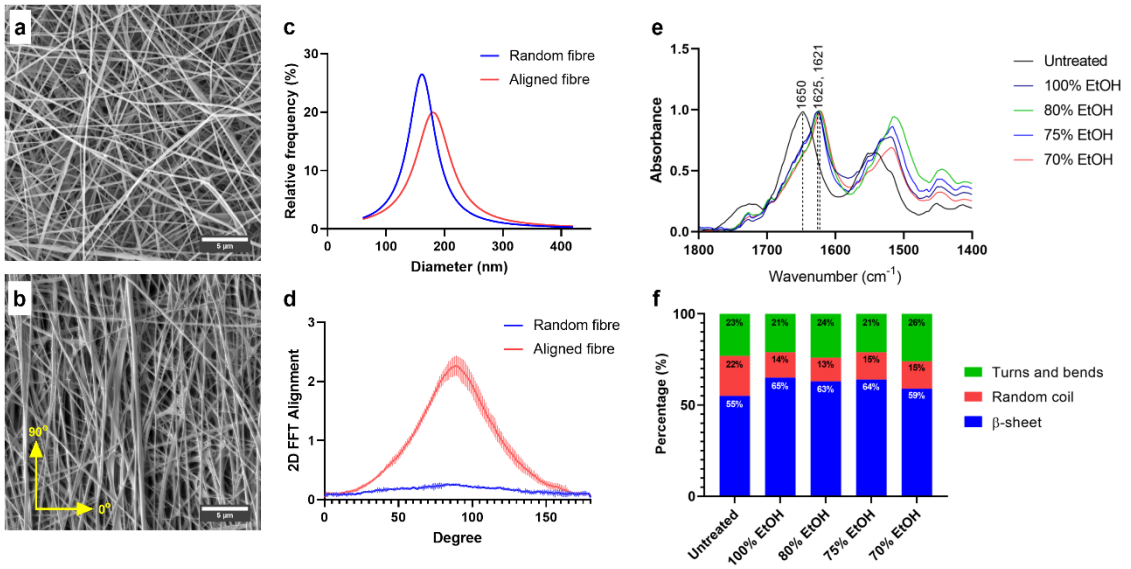

333

334 *Figure 1 Characterisation of double layer electrospun silk fibroin mats: (a) and (b) SEM of random and aligned fibres*
335 *SF with the scale bar of 5 µm and the orientation of 90º following the Cartesian coordinate system, (c) distribution of*
336 *fibre diameters, (d) 2D FFT alignment of fibres measured from 3 samples (3 independent electrospinning*
337 *experiments), (e) ATR-FTIR spectra of amide I band (1700 – 1600 cm^{-1}), and (f) the relative percentages of secondary*
338 *protein structures of electrospun SF after ethanol treatment.*

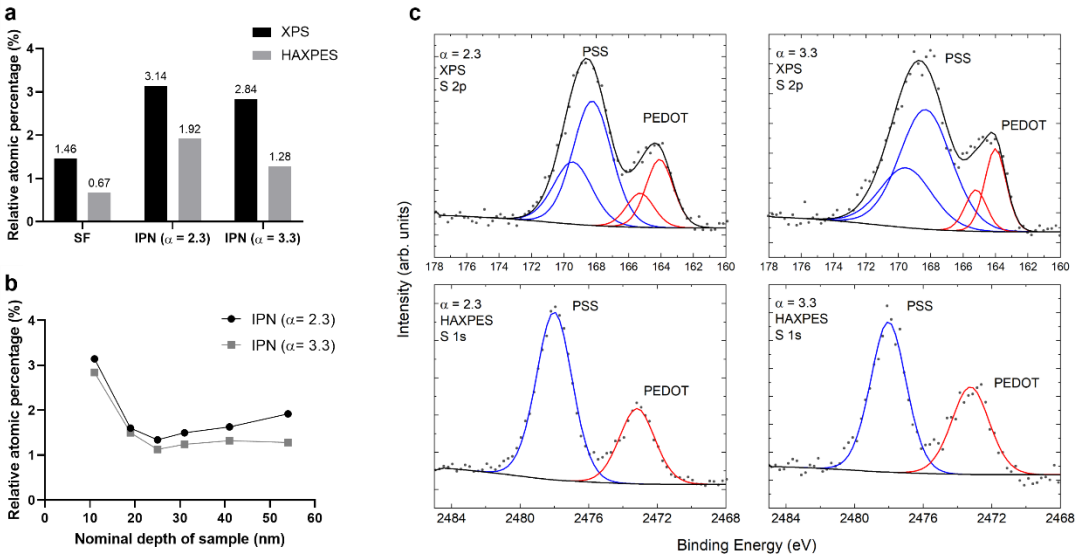

339

340 *Figure 2 surface-sensitive XPS and bulk-sensitive HAXPES analysis of electrospun SF, IPN (α = 2.3), and IPN (α =*
341 *3.3): (a) relative percentage of S compared to total elements (C,O, and N), (b) relative percentage of S of IPN mats*
342 *at different depths of sample, and (c) comparison of XPS and HAXPES spectra for S in the IPN mats. The S 2p and S*
343 *1s core levels are used for XPS and HAXPES measurements respectively, with sampling depths of ~11 and 54 nm.*

3.2 Electrical properties of electrospun SF and IPNs

The electrochemical properties of the materials were studied via cyclic voltammetry (CV) and electrical impedance spectroscopy (EIS), shown in Figure 3. CV was used to study the reduction/oxidation processes and electron-transfer properties of the IPNs; voltammograms of the materials show an anodic peak at ca. -0.2 V and the corresponding cathodic peak at ca. -0.6 V vs a Ag/AgCl reference electrode analogous to the literature [68] the somewhat unsymmetrical cathodic/anodic peaks are likely to be due to differences in background current and kinetic limitations [69, 70]. The Nyquist plots derived from EIS also showed semicircle curves in the high-frequency range due to electron-transfer resistance (R_{et}) of the materials, calculated by the difference of the real axis of impedance [71], and the vertical line that follows along the imaginary axis corresponds to a diffusion process. The R_{et} of IPN ($\alpha = 2.3$) and IPN ($\alpha = 3.3$) were ca. 330 Ω and 350 Ω, respectively suggesting the homogeneous coating of the materials with PEDOT:PSS. The electrical conductivity of pristine SF was ca. $\times 10^{-8}$ S/m, while those of IPN materials were ca. $\times 10^{-4}$ to 10^{-3} S/m (Supplementary information, table S2).

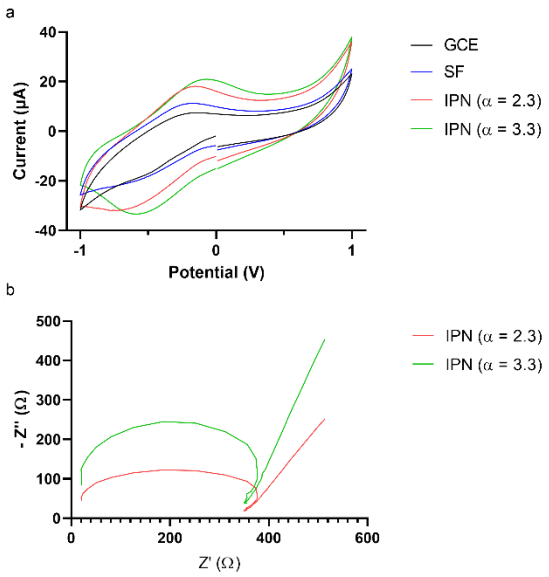

358

359 *Figure 3 Electrochemical characterisation of electrospun SF and IPN materials: (a) cyclic voltammetry (CV) data*
360 *and (b) Nyquist plots derived from electrochemical impedance spectroscopy (EIS).*

3.3 Mechanical properties of electrospun SF and IPNs materials

Electrospun SF mats are very fragile when they are dry. The ultimate tensile stress was 1.41 ± 0.21 MPa, the strain at break was 3 ± 1%, Young's modulus was 43.3 ± 16.8 MPa, and toughness was 12.7 ± 1.47 kJ/m^3. After ethanol treatment, the ultimate tensile stress was significantly increased to 2.62 ± 0.49 MPa but the strain was similar resulting in the higher Young's modulus as shown in the Figure 4. However, it is noteworthy that the mechanical properties of the electrospun SF are completely changed when the materials are soaked in water overnight, after which, the ultimate tensile stress was decreased to 0.87 ± 0.26 MPa while the strain was increased to 12 ± 2% indicating that these materials are more flexible in the wet state. For the IPNs (α = 2.3 and 3.3) mats in the wet state their stresses, strains, and toughness are slightly decreased from the wet state electrospun SF.

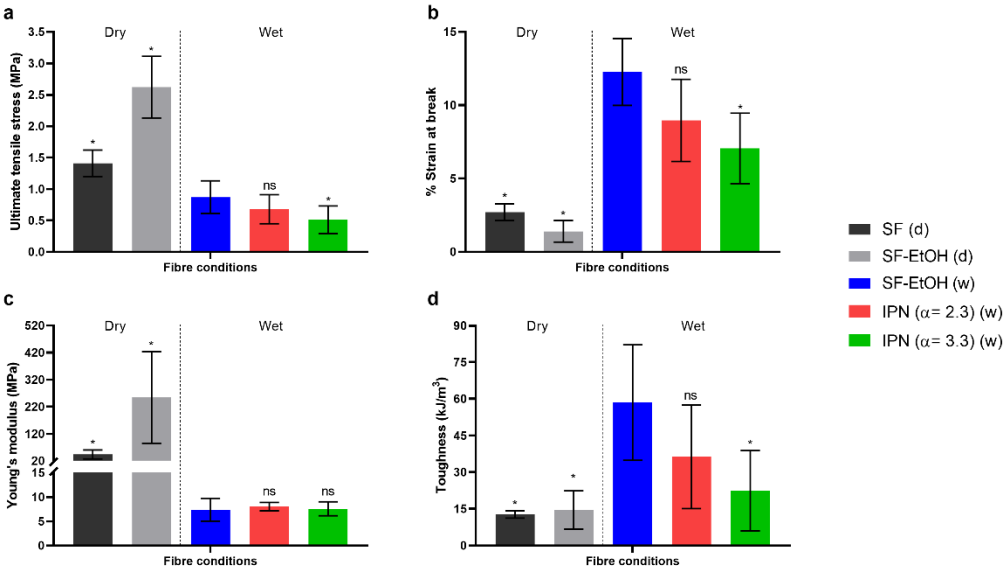

*Figure 4 Mechanical properties of electrospun SF and IPN mats in dry and wet states: (a) ultimate tensile stress, (b) % strain at break, (c) Young's modulus, and (d) toughness. All plotted with mean and SD. * represents the significant difference from the wet state ethanol-treated electrospun SF (Blue group), tested by One-Way ANOVA (Dunnett) with P-value ≤ 0.01. The n number represents the number of samples from three independent electrospinning experiments: SF (d) – (n = 3), SF-EtOH (d) – (n = 3), SF-ETOH (w) – (n = 9), IPN (α = 2.3) (w) – (n = 9), and IPN (α = 3.3) (w) – (n = 8).*

3.4 In silico toxicity and in vitro cytotoxicity studies

The safety data sheets for the starting materials and products (PEDOT-PSS for the dip-coating method; or EDOT, PSS, sodium persulfate and iron (II) sulfate heptahydrate for the IPN method) show PSS and PEDOT-PSS to be non-hazardous (according to Regulation (EC) No. 1272/2008), EDOT to be a toxic irritant, sodium persulfate to be a toxic sensitizer, and iron (II) sulfate heptahydrate to be a toxic irritant, highlighting the importance of effective washing prior to contemplating any biomedical applications. *In silico* toxicity screening of the various components was carried out using Derek Nexus [72] Derek Nexus: v. 6.0.1, Nexus: 2.2.2) and Sarah Nexus [73] (Sarah Nexus: v. 3.0.0, Sarah Model: 2.0) that can be used to assess the potential biocompatibility of materials (Derek identifies structural alerts for several endpoints and Sarah is a statistical-based model focused on mutagenicity only).[74-76] *In silico* toxicity screening studies showed PEDOT, PSS and PEDOT-PSS were non-sensitizers and non-mutagenic; however, formic acid was identified as an irritant by Derek Nexus, EDOT was identified as plausibly hepatotoxic by Derek Nexus, and sodium persulfate was identified as a plausible respiratory/skin sensitizer by Derek Nexus, reinforcing the importance of effective washing prior to contemplating any biomedical applications.

The pH of the extracted cell culture medium of electrospun SF and IPNs (α = 2.3 and 3.3) was approximately 7.8, similar to the normal growth medium, demonstrating no residual acidic components leaching from the materials (and importantly, the efficiency of the sample preparation). Subconfluent NG108-15 cells on glass substrates exposed to these extracted media can grow and proliferate slowly, confirmed by the DNA concentration result as shown in Figure 5a. Importantly, the DNA concentrations of NG108-15 after exposure to extracted media gradually increased over time, although they were slightly lower than the control condition, NG108-15

cultured on tissue culture plastic (TCP) with the normal growth medium; these subtle differences in the first few days are accounted for by surface chemistry and time taken for the cells to produce their own extracellular matrices.

The live/dead staining reveals that the cell morphology is slightly changed after exposure by the extracted media. Live cells and dead cells are stained in green and red respectively as shown in Figure 5b – e. Commonly, NG108-15 grow individually and evenly spread all over the area. Each cell can extend small neurites from its cell body. There are more clusters of rounded cells once cultured with extracted media especially from IPN conditions as shown in the Figure 5d and 5e.

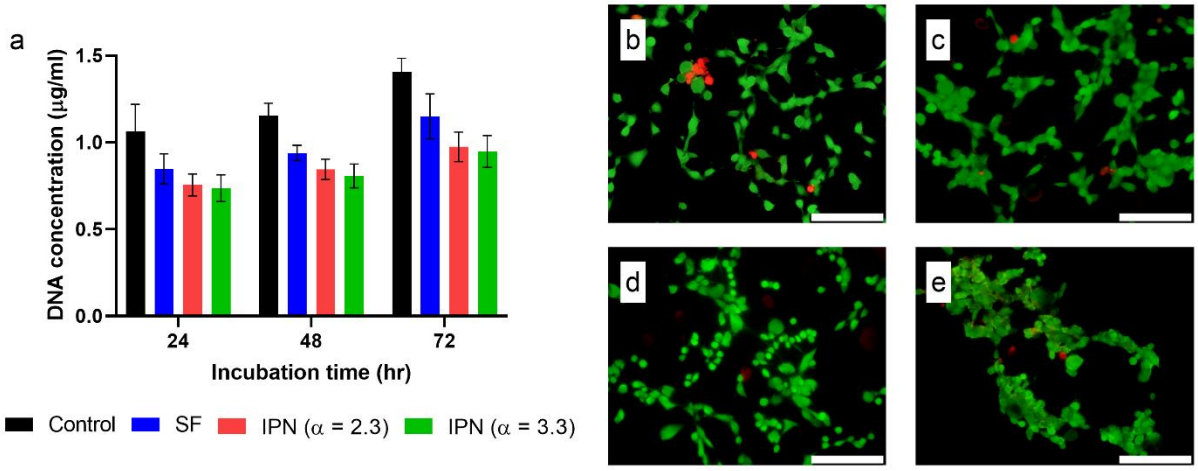

Figure 5 NG108-15 grown on TCP with the extracted media (conditioned media): (a) DNA concentration of NG108-15 cultured in normal growth medium, extracted medium of electrospun SF and IPNs (α = 2.3 and 3.3) for 24 – 72 hr, (n=3) no significant different between SF and IPNs groups. The live/dead staining of NG 108-15 on glass substrates after incubated with (b) normal growth medium, (c) extracted medium of electrospun SF, (d) extracted medium of IPN (α = 2.3), and (e) extracted medium of IPN (α = 3.3) at 72 hr with the scale bar of 150 µm.

3.5 neuron growth, neurite extension and orientation

In accordance with results of the media-extraction assay, live/dead staining suggested that the electrospun SF and IPNs mats were biocompatible without toxicity from any chemical residue eluting from the IPNs. In the direct contact assay, NG108-15 grown on electrospun SF and IPNs mats were examined by the metabolic activity and DNA concentration. Previous studies showed that metabolic activity correlated with cell viability [48, 49]; thus, it was used in the direct test instead of the live/dead staining, and the morphology of cells on fibres was observed using SEM and immunofluorescence.

The metabolic activity and DNA concentration profiles of NG108-15 directly cultured on uncoated substrates and laminin coated substrates are similar (Figure 6). Typically, the metabolic activity was observed to increase from ~50 to 1200 A.U., and the DNA concentration was observed to increase from ~0.1 to 0.5 µg/mL over the period of 7 days. The metabolic activity of the electrospun SF condition was significantly higher than that of IPN ($\alpha = 3.3$) at day 5, but similar at day 7. Additionally, the DNA concentration of the electrospun SF condition was higher than that of IPN ($\alpha = 2.3$ and 3.3) at day 3 and 5, while they are similar at day 7 as well.

Furthermore, SEM results support the observation that NG108-15 can grow and extend their neurites on electrospun SF and IPNs materials for 7 days, even though they were cultured without the differentiation factor, cAMP. We observe that neurite extension lengths on the laminin coated materials are slightly longer than on uncoated materials (Supplementary information, Figure S7). Although the average neurite lengths are similar (around 30 – 40 µm) for all conditions and substrates, the 90^{th} percentiles of the neurite lengths are different. Neurite lengths are 55, 45, and

50 µm on laminin coated electrospun SF, IPN ($\alpha = 2.3$), and IPN ($\alpha = 3.3$), while, they are 35, 50, and 40 µm on uncoated electrospun SF, IPN ($\alpha = 2.3$), and IPN ($\alpha = 3.3$), respectively.

In the differentiation phase of NG108-15, cells are grown as clusters and extend many more longer neurites compared to the normal growth phase as shown in Figure 7. The immunofluorescence confirms the processes extended from the cell clusters are neurites due to the β-III tubulin staining. The average neurite length in this phase is ~80 µm for all conditions. Interestingly, most neurites are orientated in the parallel direction to the fibre alignment (evidence of the instructive nature of the topological cues imparted by fibre alignment), which is in the position of 90^{o} in the polar-plots of Figure 8. The maximum neurite lengths reach to 300 µm in the condition of laminin coated electrospun SF and laminin coated IPN ($\alpha = 2.3$). The other conditions have the maximum neurite length of ~200 – 250 µm. The 90^{th} percentiles of the neurite length are ~120 – 140 µm in all condition except laminin coated electrospun SF, which is 180 µm.

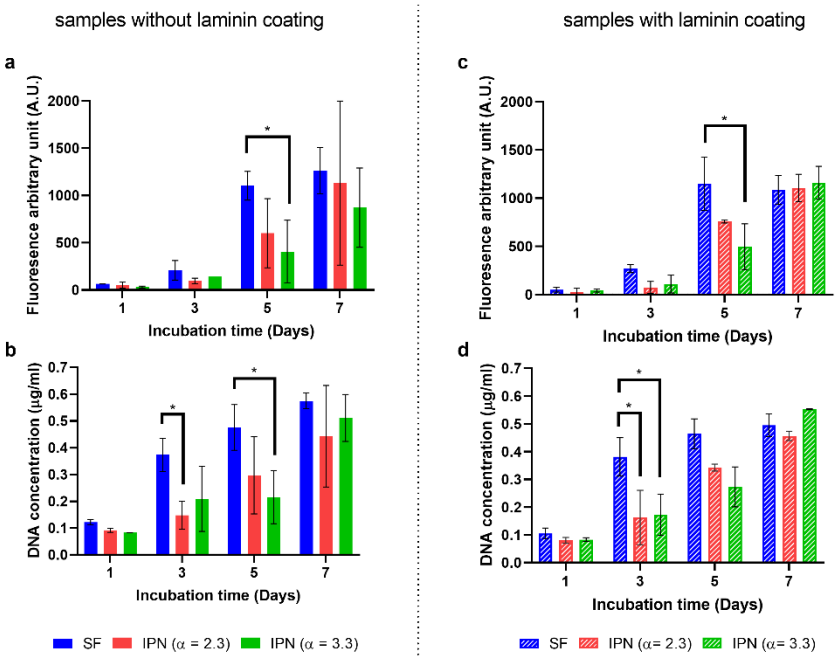

449

450 *Figure 6 <u>In vitro</u> biocompatibility results of NG108-15 directly cultured on electrospun SF and IPNs mats for 7 days:*
451 *(a) cell metabolic activity and (b) DNA concentration of uncoated substrates. (c) cell metabolic activity and (d) DNA*
452 *concentration of laminin-coated substrates, * represents the significant difference via Tukey's multiple comparisons*
453 *test comparing to SF as a control with P value ≤ 0.03, (n = 3 independent samples).*

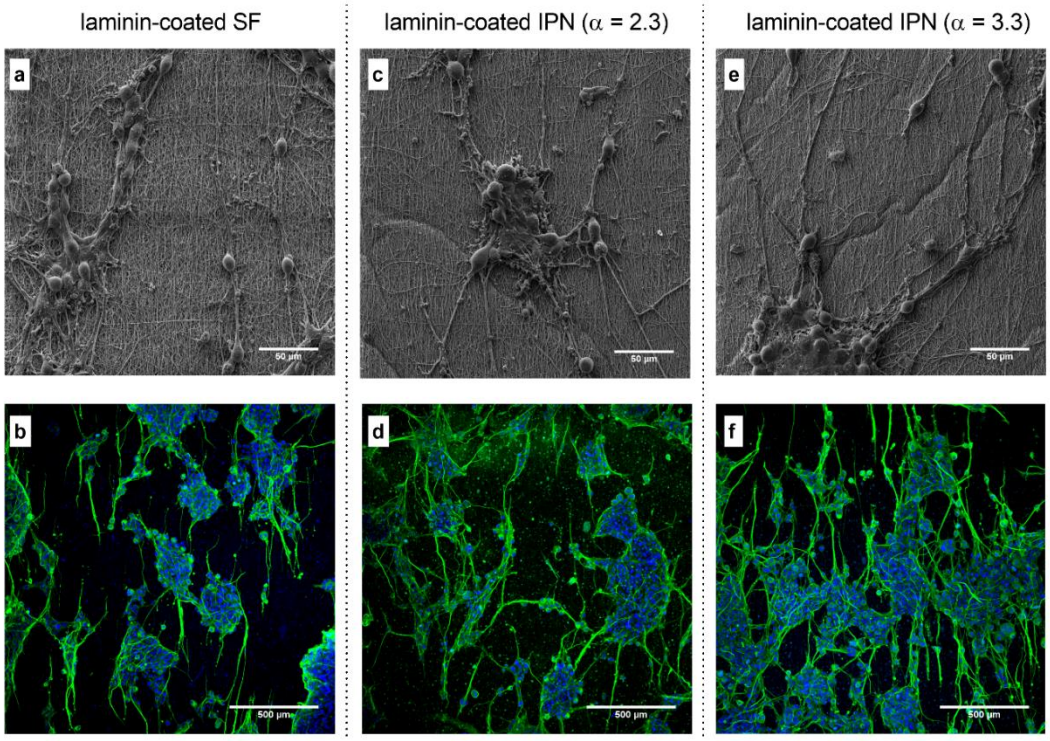

454

455 *Figure 7 SEM and immunofluorescence staining of differentiated NG108-15 on laminin coated electrospun SF and*
456 *IPNs mats. The alignment of fibres is at 90º following the Cartesian coordinate system. The nuclei are stained with*
457 *DAPI (blue) and the β-III tubulin representing neurites are stained with Alexa Fluor® 488 (green).*

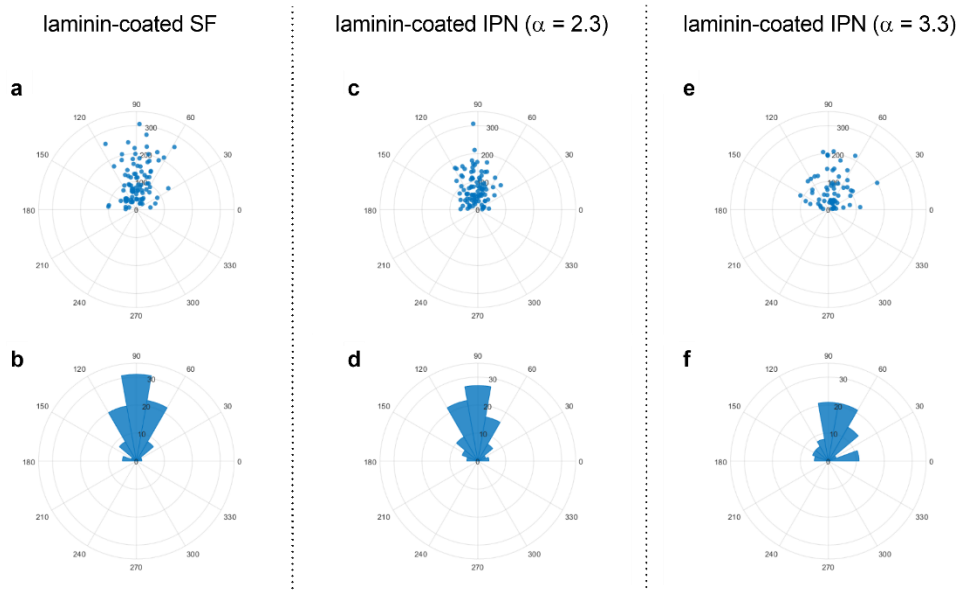

458

459 *Figure 8 Neurite orientation and length of differentiated NG108-15 on laminin-coated electrospun SF and IPNs mats*
460 *at day 7: (a, c, and d) the polarscatters of neurites oriented in the different angles, the radius represents the length of*
461 *neurite (µm). (b, d, and f) the polarhistogram of neurites, the radius represents the relative percentage of number of*
462 *neurites aligned in the different angles from 0º – 180º with the bin width of 20°.*

4. Discussion

4.1 Novel method for electrospinning SF and PEDOT:PSS modification

Commonly, the preparation of SF from silk cocoons requires 4 sequential steps: degumming, dissolution, dialysis, and either lyophilisation followed by more processing [18] or film casting followed by more processing [77, 78]. There are two well known protocols using aqueous solvents, LiBr solution [18] and $CaCl_2$/ethanol/water [79] to dissolve the degummed SF, both of which disrupt the β-sheets present in the silk fibroin fibres within a few hours, and require dialysis thereafter. Dialysis is time-consuming and potentially complicated by gelation during dialysis, and to avoid these complications we prepared the electrospinning SF solution via a dialysis free protocol using a non-aqueous solvent system.

SF can be processed in various non-aqueous solvent systems, including FA [78, 80-82], hexafluoroisopropanol (HFIP) [83], dichloromethane (DCM) [84], etc.; FA with the addition of $CaCl_2$ can dissolve degummed SF within 3 h, enabling film casting and subsequent re-dissolution for electrospinning later [85]. This led to the idea of preparing electrospinning SF without the casting/redissolution in FA/$CaCl_2$, yielding fibres with diameters of ~200 nm.

The electrospun SF can be rendered conductive either via dip coating or via growth of an IPN of PEDOT:PSS in/on the electrospun SF, as assessed visually (by color change from off white to blue) and confirmed by HAXPES (showing higher %S especially at the surface of material, ~11 nm). The S1 s spectra show the same ratio between PSS and PEDOT peaks at all depths of the IPNs. The higher S content of IPNs than on dip coated materials is likely due to the non-covalent adsorption of PEDOT:PSS on SF during dip coating is significantly weaker than the covalent bonds formed during IPN formation between the EDOT and aromatic amino acids on SF.

4.2 Flexibility and electrical conductivity of electrospun SF

The formation of β-sheets in the electrospun SF after ethanol treatment increases the mechanical properties. In the wet state, the electrospun materials are more flexible than in the dry state due to the plasticization of the SF chains by water [86]. The IPNs are all somewhat weaker than the electrospun SF alone which is likely to be due to disruption of hydrogen bonding between the protein chains after growth of the IPN.

The electrical conductivity of the SF/PEDOT:PSS IPN materials (ca. 10^{-4} to 10^{-3} S/m) shows they are semiconductors (similar to the literature [26, 87]), while the pristine SF is an insulator [24-26]. In a previous study of our groups, the conductivity of SF/PEDOT:PSS prepared via another coating technique was also in the range of semiconductors ($\times10^{-3}$ to 10^{1} S/m), influenced by the concentration of PEDOT:PSS [48], which highlights the effects of subtly different processing on the properties of the electroactive biomaterials.

4.3 Effects of PEDOT:PSS on the neural growth

PEDOT:PSS can promote neurogenic differentiation and the expression of β-III tubulin in neurites [38]. The in silico toxicity study suggests any residues from the preparation and processing of electrospun SF and IPNs may hinder cell growth, however, thorough washing minimized such complications. In vitro studies using NG108-15 cells indicate their aggregation as clusters without high levels of dead cells once cultured with the extracted medium of IPNs mats, pH = 7.8. Interestingly, more cell clusters were observed on the conductive IPNs than the non-conductive electrospun SF regardless of whether they were coated with laminin or not, suggesting subtle differences in cell-material interactions are important for cell differentiation; [88] and that cell

aggregates were also observed when NG108-15 cells were cultured with the differentiation medium as well (Supplementary information, S8).

4.4 Neurites extension and orientation on sub-micron aligned fibres

A previous study using analogous nanofibrous SF/PEDOT:PSS-based biomaterials were shown to adsorb more protein (Bovine serum albumin) than pristine SF [48], and proteins such as gelatin have been used to render PEDOT-based biomaterials more cell adhesive [89]. In this study the IPNs were coated with a thin layer of adsorbed laminin (akin to other studies where laminin was used to coat electrodes for cell culture with small changes to impedance [90] and no significant changes in the electrochemical properties of the electrodes [91]), however, quantification of laminin adsorbtion on such complex hydrophilic nanofibrous IPNs is not reproducibly measurable. The laminin-coating of all substrates was used to enhance cell adhesion and promote the neurite length. There is a small increase of neurite length ~10 μm on laminin-coated substrates but no significant difference between electrospun SF and the IPNs. These results suggest that the conductive IPN biomaterials induce cell aggregation which is involved in cell differentiation [88].

In the differentiation phase, a cluster of cells extends neurites with increased lengths compared to the growth phase. Most neurites are oriented parallel to the fibre alignment of electrospun SF, confirming the sub-micron aligned electrospun SF can control the direction of neurite extension. Moreover, the laminin-coated substrates promote longer neurites. The average length of neurite on laminin-coated electrospun SF and IPNs are similar; however, it is noteworthy that the longest neurite outgrowth of 300 μm was observed in the parallel direction of fibre alignment on laminin-coated electrospun SF and IPN ($\alpha = 2.3$) mats, which is also the material with the lowest electron

transfer resistance (R_{et}, ca. 330 Ω). This suggests that PEDOT:PSS is a supportive factor for neural differentiation but it has no crucial effects on neurite outgrowth compared to cAMP and laminin.

5. Conclusion

This novel fabrication method of double layer electrospinning SF can produce sub-micron fibres with aligned fibres to direct axon orientation. The electrospun SF material is brittle in the dry state and more flexible in the wet state due to water plasticization. Once coated with laminin, both electrospun SF and IPN materials promote the similar length of neurite extension. These developed materials, IPN of PEDOT:PSS on/in electrospun SF is novel, potentially enabling electrical stimulation of the cells and facilitating peripheral nerve regeneration.

6. Acknowledgements

This work was supported by the Henry Royce Institute for Advanced Materials, funded through EPSRC grants EP/R00661X/1, EP/P025021/1 and EP/P025498/1. We thank Zara L. Smith at University of Manchester for assistance with immunofluorescence staining, Garry R. Harper and Vasileios K. Oikonomou at Lancaster University for assistance with early attempts at silk processing. We also thank the Royal Thai Government Scholarship for support of C.P., the EPSRC (EP/R512564/1, 2065445) for support of M.D.A. and J.G.H., the BBSRC (grant BB/L0137971/1) for support of G.R.H. and J.G.H., and the British Council of Greece for the IELTS Award 2017 for support of V.K.O.

7. References

[1] K. Haastert-Talini, C. Grothe, Electrical Stimulation for Promoting Peripheral Nerve Regeneration, International Review of Neurobiology, Elsevier Inc.2013, pp. 111-124.

[2] R.M. Meadows, D.R. Sengelaub, K.J. Jones, Chapter 29 - Cellular Aspects of Nerve Injury and Regeneration A2 - Tubbs, R. Shane, in: E. Rizk, M.M. Shoja, M. Loukas, N. Barbaro, R.J. Spinner (Eds.), Nerves and Nerve Injuries, Academic Press, San Diego, 2015, pp. 433-449.

[3] A. Faroni, S.A. Mobasseri, P.J. Kingham, A.J. Reid, Peripheral nerve regeneration: experimental strategies and future perspectives, Adv Drug Deliv Rev 82-83 (2015) 160-7.

[4] R. Zhang, J.M. Rosen, The role of undifferentiated adipose-derived stem cells in peripheral nerve repair, Neural Regen Res 13(5) (2018) 757-763.

[5] Y. Sowa, T. Kishida, T. Imura, T. Numajiri, K. Nishino, Y. Tabata, O. Mazda, Adipose-Derived Stem Cells Promote Peripheral Nerve Regeneration In Vivo without Differentiation into Schwann-Like Lineage, Plast Reconstr Surg 137(2) (2016) 318e-330e.

[6] A.N. Leberfinger, D.J. Ravnic, R. Payne, E. Rizk, S.V. Koduru, S.W. Hazard, Adipose-Derived Stem Cells in Peripheral Nerve Regeneration, Curr Surg Rep 5(2) (2017).

[7] K. Haastert-Talini, C. Grothe, Chapter Five - Electrical Stimulation for Promoting Peripheral Nerve Regeneration, in: S. Geuna, I. Perroteau, P. Tos, B. Battiston (Eds.), International Review of Neurobiology, Academic Press2013, pp. 111-124.

[8] Y.S. Chen, C.L. Hu, C.L. Hsieh, J.G. Lin, C.C. Tsai, T.H. Chen, C.H. Yao, Effects of percutaneous electrical stimulation on peripheral nerve regeneration using silicone rubber chambers, J Biomed Mater Res 57(4) (2001) 541-549.

[9] C.H. Yao, R.L. Chang, S.L. Chang, C.C. Tsai, F.J. Tsai, Y.S. Chen, Electrical stimulation improves peripheral nerve regeneration in streptozotocin-induced diabetic rats, J Trauma Acute Care 72(1) (2012) 199-205.

[10] J.H. Huang, L. Lu, X.Y. Hu, Z.X. Ye, Y. Peng, X.D. Yan, D. Geng, Z.J. Luo, Electrical Stimulation Accelerates Motor Functional Recovery in the Rat Model of 15-mm Sciatic Nerve Gap Bridged by Scaffolds With Longitudinally Oriented Microchannels, Neurorehab Neural Re 24(8) (2010) 736-745.

[11] J.G. Hardy, Z.Z. Khaing, S.J. Xin, L.W. Tien, C.E. Ghezzi, D.J. Mouser, R.C. Sukhavasi, R.C. Preda, E.S. Gil, D.L. Kaplan, C.E. Schmidt, Into the groove: instructive silk-polypyrrole films with topographical guidance cues direct DRG neurite outgrowth, J Biomat Sci-Polym E 26(17) (2015) 1327-1342.

[12] S. Das, M. Sharma, D. Saharia, K.K. Sarma, E.M. Muir, U. Bora, Electrospun silk-polyaniline conduits for functional nerve regeneration in rat sciatic nerve injury model, Biomed Mater 12(4) (2017).

[13] J.Y. Lee, C.A. Bashur, A.S. Goldstein, C.E. Schmidt, Polypyrrole-coated electrospun PLGA nanofibers for neural tissue applications, Biomaterials 30(26) (2009) 4325-35.

[14] M.P. Prabhakaran, L. Ghasemi-Mobarakeh, G.R. Jin, S. Ramakrishna, Electrospun conducting polymer nanofibers and electrical stimulation of nerve stem cells, J Biosci Bioeng 112(5) (2011) 501-507.

[15] J.G. Hardy, R.C. Cornelison, R.C. Sukhavasi, R.J. Saballos, P. Vu, D.L. Kaplan, C.E. Schmidt, Electroactive Tissue Scaffolds with Aligned Pores as Instructive Platforms for Biomimetic Tissue Engineering, Bioengineering-Basel 2(1) (2015) 15-34.

[16] A. Magaz, A.D. Roberts, S. Faraji, T.R.L. Nascimento, E.S. Medeiros, W.Z. Zhang, R.D. Greenhalgh, A. Mautner, X. Li, J.J. Blaker, Porous, Aligned, and Biomimetic Fibers of Regenerated Silk Fibroin Produced by Solution Blow Spinning, Biomacromolecules 19(12) (2018) 4542-4553.

[17] A. Magaz, A. Faroni, J.E. Gough, A.J. Reid, X. Li, J.J. Blaker, Bioactive Silk-Based Nerve Guidance Conduits for Augmenting Peripheral Nerve Repair, Adv Healthc Mater 7(23) (2018).

[18] D.N. Rockwood, R.C. Preda, T. Yucel, X.Q. Wang, M.L. Lovett, D.L. Kaplan, Materials fabrication from Bombyx mori silk fibroin, Nat Protoc 6(10) (2011) 1612-1631.

[19] C.Z. Zhou, F. Confalonieri, M. Jacquet, R. Perasso, Z.G. Li, J. Janin, Silk fibroin: Structural implications of a remarkable amino acid sequence, Proteins 44(2) (2001) 119-122.
[20] G.H. Altman, F. Diaz, C. Jakuba, T. Calabro, R.L. Horan, J.S. Chen, H. Lu, J. Richmond, D.L. Kaplan, Silk-based biomaterials, Biomaterials 24(3) (2003) 401-416.
[21] B. Kundu, R. Rajkhowa, S.C. Kundu, X.G. Wang, Silk fibroin biomaterials for tissue regenerations, Adv Drug Deliver Rev 65(4) (2013) 457-470.
[22] M. Dodel, N.H. Nejad, S.H. Bahrami, M. Soleimani, L.M. Amirabad, H. Hanaee-Ahvaz, A. Atashi, Electrical stimulation of somatic human stem cells mediated by composite containing conductive nanofibers for ligament regeneration, Biologicals 46 (2017) 99-107.
[23] S. Aznar-Cervantes, J.G. Martinez, A. Bernabeu-Esclapez, A.A. Lozano-Perez, L. Meseguer-Olmo, T.F. Otero, J.L. Cenis, Fabrication of electrospun silk fibroin scaffolds coated with graphene oxide and reduced graphene for applications in biomedicine, Bioelectrochemistry 108 (2016) 36-45.
[24] C. Jang, j.k. Park, G.-H. Yun, H.H. Choi, H.-J. Lee, J.-G. Yook, Radio-Frequency/Microwave Gas Sensors Using Conducting Polymer, Materials 13 (2020) 2859.
[25] T.-H. Le, Y. Kim, H. Yoon, Electrical and Electrochemical Properties of Conducting Polymers, Polymers 9 (2017) 150.
[26] G. Kaur, R. Adhikari, P. Cass, M. Bown, P. Gunatillake, Electrically conductive polymers and composites for biomedical applications, RSC Advances 5(47) (2015) 37553-37567.
[27] R. Yadav, R. Purwar, Influence of metal oxide nanoparticles on morphological, structural, rheological and conductive properties of mulberry silk fibroin nanocomposite solutions, Polymer Testing 93 (2021) 106916.
[28] Q. Sun, B. Qian, K. Uto, J. Chen, X. Liu, T. Minari, Functional biomaterials towards flexible electronics and sensors, Biosensors and Bioelectronics 119 (2018) 237-251.
[29] R. Ranjana, N. Parushuram, K.S. Harisha, S. Asha, B. Narayana, M. Mahendra, Y. Sangappa, Fabrication and characterization of conductive silk fibroin–gold nanocomposite films, Journal of Materials Science: Materials in Electronics 31(1) (2020) 249-264.
[30] J.G. Hardy, S.A. Geissler, D. Aguilar, M.K. Villancio-Wolter, D.J. Mouser, R.C. Sukhavasi, R.C. Cornelison, L.W. Tien, R.C. Preda, R.S. Hayden, J.K. Chow, L. Nguy, D.L. Kaplan, C.E. Schmidt, Instructive Conductive 3D Silk Foam-Based Bone Tissue Scaffolds Enable Electrical Stimulation of Stem Cells for Enhanced Osteogenic Differentiation, Macromol Biosci 15(11) (2015) 1490-1496.
[31] B.B. Sun, T. Wu, J. Wang, D.W. Li, J. Wang, Q. Gao, M.A. Bhutto, H. El-Hamshary, S.S. Al-Deyab, X.M. Mo, Polypyrrole-coated poly(L-lactic acid-co-epsilon-caprolactone)/silk fibroin nanofibrous membranes promoting neural cell proliferation and differentiation with electrical stimulation, J Mater Chem B 4(41) (2016) 6670-6679.
[32] S. Aznar-Cervantes, A. Pagan, J.G. Martinez, A. Bernabeu-Esclapez, T.F. Otero, L. Meseguer-Olmo, J.I. Paredes, J.L. Cenis, Electrospun silk fibroin scaffolds coated with reduced graphene promote neurite outgrowth of PC-12 cells under electrical stimulation, Mat Sci Eng C-Mater 79 (2017) 315-325.
[33] S. Tsukada, H. Nakashima, K. Torimitsu, Conductive Polymer Combined Silk Fiber Bundle for Bioelectrical Signal Recording, Plos One 7(4) (2012).
[34] R.K. Pal, A.A. Farghaly, C.Z. Wang, M.M. Collinson, S.C. Kundu, V.K. Yadavalli, Conducting polymer-silk biocomposites for flexible and biodegradable electrochemical sensors, Biosens Bioelectron 81 (2016) 294-302.
[35] H.S. Park, S.J. Ko, J.S. Park, J.Y. Kim, H.K. Song, Redox-active charge carriers of conducting polymers as a tuner of conductivity and its potential window, Sci Rep-Uk 3 (2013).
[36] A.V. Volkov, K. Wijeratne, E. Mitraka, U. Ail, D. Zhao, K. Tybrandt, J.W. Andreasen, M. Berggren, X. Crispin, I.V. Zozoulenko, Understanding the Capacitance of PEDOT:PSS, Adv Funct Mater 27(28) (2017).

[37] M. Anderson, N.B. Shelke, O.S. Manoukian, X. Yu, L.D. McCullough, S.G. Kumbar, Peripheral Nerve Regeneration Strategies: Electrically Stimulating Polymer Based Nerve Growth Conduits, Crit Rev Biomed Eng 43(2-3) (2015) 131-59.
[38] S. Sirivisoot, R. Pareta, B.S. Harrison, Protocol and cell responses in three-dimensional conductive collagen gel scaffolds with conductive polymer nanofibres for tissue regeneration, Interface Focus 4(1) (2014).
[39] J.A. Sierra-Fonseca, O. Najera, J. Martinez-Jurado, E.M. Walker, A. Varela-Ramirez, A.M. Khan, M. Miranda, N.S. Lamango, S. Roychowdhury, Nerve growth factor induces neurite outgrowth of PC12 cells by promoting Gbetagamma-microtubule interaction, BMC Neurosci 15 (2014) 132.
[40] P. Moroder, M.B. Runge, H. Wang, T. Ruesink, L. Lu, R.J. Spinner, A.J. Windebank, M.J. Yaszemski, Material properties and electrical stimulation regimens of polycaprolactone fumarate-polypyrrole scaffolds as potential conductive nerve conduits, Acta Biomater 7(3) (2011) 944-53.
[41] H.T. Nguyen, S. Sapp, C. Wei, J.K. Chow, A. Nguyen, J. Coursen, S. Luebben, E. Chang, R. Ross, C.E. Schmidt, Electric field stimulation through a biodegradable polypyrrole-co-polycaprolactone substrate enhances neural cell growth, J Biomed Mater Res A 102(8) (2014) 2554-64.
[42] T. Fukazawa, M. Matsumoto, T. Imura, E. Khalesi, T. Kajiume, Y. Kawahara, K. Tanimoto, L. Yuge, Electrical stimulation accelerates neuromuscular junction formation through ADAM19/neuregulin/ErbB signaling in vitro, Neurosci Lett 545 (2013) 29-34.
[43] J.A. Doebler, Effects of neutral ionophores on membrane electrical characteristics of NG108-15 cells, Toxicol Lett 114(1-3) (2000) 27-38.
[44] J.A. Doebler, Effects of protonophores on membrane electrical characteristics in NG108-15 cells, Neurochem Res 25(2) (2000) 263-8.
[45] M.C. Acosta-García, I. Morales-Reyes, A. Jiménez-Anguiano, N. Batina, N.P. Castellanos, R. Godínez-Fernández, Simultaneous recording of electrical activity and the underlying ionic currents in NG108-15 cells cultured on gold substrate, Heliyon 4(2) (2018) e00550.
[46] M.K. Gheith, T.C. Pappas, A.V. Liopo, V.A. Sinani, B.S. Shim, M. Motamedi, J.P. Wicksted, N.A. Kotov, Stimulation of Neural Cells by Lateral Currents in Conductive Layer-by-Layer Films of Single-Walled Carbon Nanotubes, Advanced Materials 18(22) (2006) 2975-2979.
[47] K. Pawar, G. Welzel, C. Haynl, S. Schuster, T. Scheibel, Recombinant Spider Silk and Collagen-Based Nerve Guidance Conduits Support Neuronal Cell Differentiation and Functionality in Vitro, ACS Applied Bio Materials 2(11) (2019) 4872-4880.
[48] A. Magaz, B.F. Spencer, J.G. Hardy, X. Li, J.E. Gough, J.J. Blaker, Modulation of Neuronal Cell Affinity on PEDOT-PSS Nonwoven Silk Scaffolds for Neural Tissue Engineering, Acs Biomater Sci Eng 6(12) (2020) 6906-6916.
[49] A. Magaz, X. Li, J.E. Gough, J.J. Blaker, Graphene oxide and electroactive reduced graphene oxide-based composite fibrous scaffolds for engineering excitable nerve tissue, Mater Sci Eng C Mater Biol Appl 119 (2021) 111632.
[50] P.J. Kingham, D.F. Kalbermatten, D. Mahay, S.J. Armstrong, M. Wiberg, G. Terenghi, Adipose-derived stem cells differentiate into a Schwann cell phenotype and promote neurite outgrowth in vitro, Exp Neurol 207(2) (2007) 267-74.
[51] D. Kraus, V. Boyle, N. Leibig, G.B. Stark, V. Penna, The Neuro-spheroid—A novel 3D in vitro model for peripheral nerve regeneration, Journal of Neuroscience Methods 246 (2015) 97-105.
[52] T. Horii, H. Hikawa, M. Katsunuma, H. Okuzaki, Synthesis of highly conductive PEDOT:PSS and correlation with hierarchical structure, Polymer 140 (2018) 33-38.
[53] D. Wilson, R. Valluzzi, D. Kaplan, Conformational transitions in model silk peptides, Biophys J 78(5) (2000) 2690-2701.
[54] J.C. Woicik, Hard X-ray Photoelectron Spectroscopy (HAXPES) Preface, Springer Ser Surf Sc 59 (2016) V-Vi.

[55] G. Panaccione, K. Kobayashi, Hard X-ray photoemission spectroscopy: Variable depth analysis of bulk, surface and interface electronic properties, Surf Sci 606(3-4) (2012) 125-129.
[56] A. Regoutz, M. Mascheck, T. Wiell, S.K. Eriksson, C. Liljenberg, K. Tetzner, B.A.D. Williamson, D.O. Scanlon, P. Palmgren, A novel laboratory-based hard X-ray photoelectron spectroscopy system, Rev Sci Instrum 89(7) (2018).
[57] B.F. Spencer, S. Maniyarasu, B. Reed, D.J.H. Cant, R. Ahumada-Lazo, A.G. Thomas, C.A. Muryn, M. Maschek, S.K. Eriksson, T. Wiell, T.-L. Lee, S. Tougaard, S.G. Shard, W.R. Flavell, Hard X-rays and inelastic background modelling extend photoelectron spectroscopy below the surface for the detection of buried layers, Applied Surface Science (2020).
[58] M.B. Trzhaskovskaya, V.G. Yarzhemsky, Dirac-Fock photoionization parameters for HAXPES applications, Atom Data Nucl Data 119 (2018) 99-174.
[59] M.B. Trzhaskovskaya, G. Yarzhemsky, Dirac-Fock photoionization parameters for HAXPES applications, Part II: Inner atomic shells, Atom Data Nucl Data 129 (2019).
[60] M.P. Seah, A Quantitative Framework for the Analysis of Surfaces by Aes and Xps, Analusis 9(5) (1981) 171-180.
[61] S. Tanuma, C.J. Powell, D.R. Penn, Calculations of Electron Inelastic Mean Free Paths .5. Data for 14 Organic-Compounds over the 50-2000 Ev Range, Surf Interface Anal 21(3) (1994) 165-176.
[62] N. Fairley, CasaXPS, http://www.casaxps.com (2019).
[63] C.E. Ayres, B.S. Jha, H. Meredith, J.R. Bowman, G.L. Bowlin, S.C. Henderson, D.G. Simpson, Measuring fiber alignment in electrospun scaffolds: a user's guide to the 2D fast Fourier transform approach, J Biomat Sci-Polym E 19(5) (2008) 603-621.
[64] H. Alhummiany, S. Rafique, K. Sulaiman, XPS Analysis of the Improved Operational Stability of Organic Solar Cells Using a V2O5 and PEDOT:PSS Composite Layer: Effect of Varied Atmospheric Conditions, J Phys Chem C 121(14) (2017) 7649-7658.
[65] H. Yan, H. Okuzaki, Effect of solvent on PEDOT/PSS nanometer-scaled thin films: XPS and STEM/AFM studies, Synthetic Met 159(21-22) (2009) 2225-2228.
[66] K.Z. Xing, M. Fahlman, X.W. Chen, O. Inganas, W.R. Salaneck, The electronic structure of poly(3,4-ethylene-dioxythiophene): studied by XPS and UPS, Synthetic Met 89(3) (1997) 161-165.
[67] S.T. Mousavi, G.R. Harper, S. Municoy, M.D. Ashton, D. Townsend, G.H.K. Alsharif, V.K. Oikonomou, M. Firlak, S. Au-Yong, B.E. Murdock, G.R. Akien, N.R. Halcovitch, S.J. Baldock, M. Fazilati, O.V. Kolosov, B.J. Robinson, M.F. Desimone, J.G. Hardy, Electroactive Silk Fibroin Films for Electrochemically Enhanced Delivery of Drugs, Macromolecular Materials and Engineering 305(6) (2020) 2000130.
[68] M. Marzocchi, I. Gualandi, M. Calienni, I. Zironi, E. Scavetta, G. Castellani, B. Fraboni, Physical and Electrochemical Properties of PEDOT:PSS as a Tool for Controlling Cell Growth, ACS Applied Materials & Interfaces 7(32) (2015) 17993-18003.
[69] N. Casado, D. Mecerreyes, Chapter 1 Introduction to Redox Polymers: Classification, Characterization Methods and Main Applications, Redox Polymers for Energy and Nanomedicine, The Royal Society of Chemistry2021, pp. 1-26.
[70] A.V. Volkov, K. Wijeratne, E. Mitraka, U. Ail, D. Zhao, K. Tybrandt, J.W. Andreasen, M. Berggren, X. Crispin, I.V. Zozoulenko, Understanding the Capacitance of PEDOT:PSS, Advanced Functional Materials 27(28) (2017) 1700329.
[71] S.A.A. Shah, M. Firlak, S.R. Berrow, N.R. Halcovitch, S.J. Baldock, B.M. Yousafzai, R.M. Hathout, J.G. Hardy, Electrochemically Enhanced Drug Delivery Using Polypyrrole Films, Materials (Basel) 11(7) (2018).
[72] D.S. Macmillan, M.L. Chilton, A defined approach for predicting skin sensitisation hazard and potency based on the guided integration of in silico, in chemico and in vitro data using exclusion criteria, Regul Toxicol Pharmacol 101 (2019) 35-47.

[73] R.S. Foster, A. Fowkes, A. Cayley, A. Thresher, A.D. Werner, C.G. Barber, G. Kocks, R.E. Tennant, R.V. Williams, S. Kane, S.A. Stalford, The importance of expert review to clarify ambiguous situations for (Q)SAR predictions under ICH M7, Genes Environ 42 (2020) 27.
[74] A. Magaz, M.D. Ashton, R.M. Hathout, X. Li, J.G. Hardy, J.J. Blaker, Electroresponsive Silk-Based Biohybrid Composites for Electrochemically Controlled Growth Factor Delivery, Pharmaceutics 12(8) (2020).
[75] M.D. Ashton, I.C. Appen, M. Firlak, N.E. Stanhope, C.E. Schmidt, W.R. Eisenstadt, B. Hur, J.G. Hardy, Wirelessly triggered bioactive molecule delivery from degradable electroactive polymer films, Polymer International 70(4) (2021) 467-474.
[76] T. Distler, C. Polley, F. Shi, D. Schneidereit, M.D. Ashton, O. Friedrich, J.F. Kolb, J.G. Hardy, R. Detsch, H. Seitz, A.R. Boccaccini, Electrically Conductive and 3D-Printable Oxidized Alginate-Gelatin Polypyrrole:PSS Hydrogels for Tissue Engineering, Adv Healthc Mater 10(9) (2021) e2001876.
[77] K. Ohgo, C.H. Zhao, M. Kobayashi, T. Asakura, Preparation of non-woven nanofibers of Bombyx mori silk, Samia cynthia ricini silk and recombinant hybrid silk with electrospinning method, Polymer 44(3) (2003) 841-846.
[78] F. Zhang, B.Q. Zuo, Z.H. Fan, Z.G. Xie, Q. Lu, X.G. Zhang, D.L. Kaplan, Mechanisms and Control of Silk-Based Electrospinning, Biomacromolecules 13(3) (2012) 798-804.
[79] A. Ajisawa, Dissolution of silk fibroin with calciumchloride/ethanol aqueous solution, The Journal of Sericultural Science of Japan 67(2) (1998) 91-94.
[80] S.H. Kim, Y.S. Nam, T.S. Lee, W.H. Park, Silk fibroin nanofiber. Electrospinning, properties, and structure, Polym J 35(2) (2003) 185-190.
[81] S. Sukigara, M. Gandhi, J. Ayutsede, M. Micklus, F. Ko, Regeneration of Bombyx mori silk by electrospinning - part 1: processing parameters and geometric properties, Polymer 44(19) (2003) 5721-5727.
[82] B.M. Min, G. Lee, S.H. Kim, Y.S. Nam, T.S. Lee, W.H. Park, Electrospinning of silk fibroin nanofibers and its effect on the adhesion and spreading of normal human keratinocytes and fibroblasts in vitro, Biomaterials 25(7-8) (2004) 1289-1297.
[83] K.H. Zhang, Q.Z. Yu, X.M. Mo, Fabrication and Intermolecular Interactions of Silk Fibroin/Hydroxybutyl Chitosan Blended Nanofibers, Int J Mol Sci 12(4) (2011) 2187-2199.
[84] J.P. Chen, S.H. Chen, G.J. Lai, Preparation and characterization of biomimetic silk fibroin/chitosan composite nanofibers by electrospinning for osteoblasts culture, Nanoscale Res Lett 7 (2012) 1-11.
[85] Z. Liu, F. Zhang, J.F. Ming, S.Y. Bie, J.J. Li, B.Q. Zuo, Preparation of Electrospun Silk Fibroin Nanofibers from Solutions Containing Native Silk Fibrils, J Appl Polym Sci 132(1) (2015).
[86] C.L. Mo, P.Y. Wu, X. Chen, Z.Z. Shao, The effect of water on the conformation transition of Bombyx mori silk fibroin, Vib Spectrosc 51(1) (2009) 105-109.
[87] H. Okuzaki, S. Takagi, F. Hishiki, R. Tanigawa, Ionic liquid/polyurethane/PEDOT:PSS composites for electro-active polymer actuators, Sensors and Actuators B: Chemical 194 (2014) 59-63.
[88] L. Laflamme, M. Gasparo, J.M. Gallo, M.D. Payet, N. Gallo-Payet, Angiotensin II induction of neurite outgrowth by AT2 receptors in NG108-15 cells. Effect counteracted by the AT1 receptors, J Biol Chem 271(37) (1996) 22729-35.
[89] J.G. Hardy, H. Li, J.K. Chow, S.A. Geissler, A.B. McElroy, L. Nguy, D.S. Hernandez, C.E. Schmidt, Conducting polymer-based multilayer films for instructive biomaterial coatings, Future Science OA 1(4) (2015).
[90] Y. Qiu, R. Liao, X. Zhang, Impedance-based monitoring of ongoing cardiomyocyte death induced by tumor necrosis factor-alpha, Biophys J 96(5) (2009) 1985-91.
[91] M.K.U. Sikder, W. Tong, H. Pingle, P. Kingshott, K. Needham, M.N. Shivdasani, J.B. Fallon, P. Seligman, M.R. Ibbotson, S. Prawer, D.J. Garrett, Laminin coated diamond electrodes for neural stimulation, Mater Sci Eng C Mater Biol Appl 118 (2021) 111454.

Instructive electroactive electrospun silk fibroin-based biomaterials for peripheral nerve tissue engineering

Chinnawich Phamornnak[a], Bing Han[a], Ben F. Spencer[a], Mark D. Ashton[d], Christopher F. Blanford[a,b,c], John G. Hardy[d,e], Jonny J. Blaker[a,f,*] Sarah H. Cartmell[a,*]

[a]Department of Materials and Henry Royce Institute, University of Manchester, Manchester, United Kingdom

[b]Manchester Institute of Biotechnology, University of Manchester, Manchester, United Kingdom

[c]National Graphene Institute, University of Manchester, Manchester, United Kingdom

[d]Department of Chemistry, Lancaster University, Lancaster, United Kingdom

[e]Materials Science Institute, Lancaster University, Lancaster, United Kingdom

[f]Department of Biomaterials, Institute of Clinical Dentistry, University of Oslo, Oslo, Norway

*Corresponding authors at: Department of Materials, University of Manchester, Sackville Street Building, Manchester, M1 3BB, United Kingdom. Tel: +44 (0) 161 306 3567. Email address: jonny.blaker@manchester.ac.uk and sarah.cartmell@manchester.ac.uk

Abstract

Aligned sub-micron fibres are an outstanding surface for orienting and promoting neurite outgrowth; therefore, attractive features to include in peripheral nerve tissue scaffolds. A new generation of peripheral nerve tissue scaffolds is under development incorporating electroactive materials and electrical regimes as instructive cues in order to facilitate full functional regeneration. Herein, electroactive fibres composed of silk fibroin (SF) and poly(3,4-ethylenedioxythiophene):polystyrene sulfonate (PEDOT:PSS) were developed as a novel

peripheral nerve tissue scaffold. Mats of SF with sub-micron diameter of 190 ± 50 nm were fabricated by double layers electrospinning with thicknesses of ~100 µm (~70 – 80 µm random fibres and ~20 – 30 µm aligned fibres). Electrospun SF mats were modified with interpenetrating polymer networks (IPN) of PEDOT:PSS in various ratios of PSS/EDOT (α) and the polymerization was assessed by hard X-ray photoelectron spectroscopy (HAXPES). The mechanical properties of electrospun SF and IPNs mats were characterized by the wet state tensile and the electrical properties were examined by cyclic voltammetry (CV) and electrochemical impedance spectroscopy (EIS). The cytotoxicity and biocompatibility of the optimal IPNs (α = 2.3 and 3.3) mats were ascertained via the growth and neurite extension of mouse neuroblastoma x rat glioma hybrid cells (NG108-15) for 7 days. The longest neurite outgrowth of 300 µm was observed in the parallel direction of fibre alignment on laminin-coated electrospun SF and IPN (α = 2.3) mats which is the material with the lowest electron transfer resistance (R_{et}, ca. 330 Ω). These electrically conductive composites with aligned sub-micron fibres exhibit promise for axon guidance and also has the potential to be combined with electrical stimulation treatment as a further step for the effective regeneration of nerves.

Keywords: Electroactive biomaterials, Electrospinning, Interpenetrating polymer network, Silk fibroin, Peripheral nerve regeneration

1. Introduction

Peripheral nerve injury (PNI) is a severe problem for trauma patients worldwide [1]. Although injured nerves can regenerate themselves, the level of functional recovery is often unsatisfactory and it is very challenging to delivery full recovery due to the limitations of neural sizes, distances, regeneration periods, etc. [2]. The most recent research trends have focused on "active" environments for regeneration such as the use of stem cells [3-6], external electrical stimulation [7-10], and electrically conductive scaffolds [11-15] in order to accelerate regenerative outcomes. One of the promising materials for developing tissue scaffolds is silk fibroin (SF) from *Bombyx mori* silk cocoons.

SF fibres are natural biocompatible materials with high mechanical strength, which can be dissolved and processed into many forms (such as films, foams, hydrogels, and fibres) [16-18]. SF is predominantly composed of heavy (H) and light (L) chain fibroins connected via disulfide bonds and glycoprotein P25. The H-chain is a repeating amino acid sequence of glycine – alanine – glycine – alanine – x, where x is serine or tyrosine [19]. The fibres have a high content of antiparallel β-sheets, hydrophobic and crystalline structures, which play a key role in the strength of the fibres, and the L-chain is a smaller hydrophilic structure [20, 21]. The electrospinning of SF has been studied for its potential application in peripheral nerve regeneration for a decade, showing promising results for neural growth and neurite extension, *in vitro* [12, 22, 23]. While electrospinning silk is time-consuming and environmentally dependent (particularly on the humidity of the spinning chamber), it produces materials with biomimetic structures. Das et al., 2017 showed that electrically conductive SF scaffolds promoted stronger action potentials at the distal end of the injured site compared to non-conductive SF scaffolds *in vivo* [12], suggesting the

electroactive SF may promote full functional nerve regeneration, and motivating the development of variants of conductive SF scaffolds for tissue engineering.

Electrical conductors, semiconductors, and insulators are defined by their conductivity. Typically conductors have conductivities from 10^4 – 10^7 S/m (e.g., metals), semiconductors from 10^{-6} – 10^4 S/m, and insulators from 10^{-20} – 10^{-10} S/m [24-26]. Logically, SF has been reported as an electrical insulator with the conductivity range of 10^{-17} – 10^{-11} S/m [27-29]. Various conductive materials including polypyrrole (PPy) [23, 30, 31], polyaniline (PANi) [12], graphene oxide (GO) [23], reduced graphene oxide (rGO) [23, 32], poly(3,4-ethylenedioxythiophene) (PEDOT) [22], and PEDOT doped with polystyrene sulfonate (PEDOT:PSS) [33, 34] have been combined with electrospun SF. These conductive materials can stably blend with SF-based materials due to the physical and non-covalent crosslinks (including hydrogen bonding and electrostatic interactions) within SF-based materials [33]. In this study, PEDOT:PSS was chosen for SF modification due to its low cost, high conductivity, high thermal stability and water solubility (facilitating processing, storage and sterilization) [35, 36], and moreover, for peripheral nerve tissue engineering applications it can support cell proliferation and promote the expression of neurogenic differentiation factors such as MAP2 and β-III tubulin [37, 38]. Furthermore, electrical stimulation through the PEDOT:PSS incorporated scaffold affects the cell alignment and enhances the length of neurite extension [37].

Even though rat adrenal pheochromocytoma cell line (PC-12) is commonly used in neural regeneration, particularly neurite outgrowth [13, 31, 32, 39-41], mouse neuroblastoma x rat glioma hybrid cell (NG108-15) is preferred in this study due to the electrophysiology. Typically, NG108-15 is used in the study of action potential of nerves [42-46]; however, many previous studies also

used NG108-15 for neuron regeneration [47-51]. Therefore, NG108-15 can use for both the neurite extension study and the functionality of the regrowth nerve via the electrophysiology. It is to be hoped that NG108-15 will be an attractive cell line for peripheral nerve regeneration, especially to study the action potential of cells grown on electrically conductive material with electrical stimulation in the future.

This study aims to develop the electrically conductive tissue scaffolds based on electrospun SF for peripheral nerve regeneration. The strategy of double layer electrospinning is designed for material reinforcement and enhancing the properties of the processed materials. The thick layer of random fibres is the base layer with a thinner layer of aligned fibres on top to instruct the direction of neurite outgrowth [11]. The novel protocol for electrospinning such mats was optimised to reduce the time-consumed by dialysis. The electrical properties of the electrospun SF mats were modified via growth of an interpenetrating polymer network (IPN) of PEDOT:PSS. The IPN mats were cultured with a neural-like cell line (NG108-15) in order to study the neural growth and neurite extension profiles on the materials. The knowledge generated by this study presents another step towards the development of a conductive scaffold leading to the successful functional recovery of peripheral nerve injuries, with the potential to apply electrical stimulation in future studies.

2. Materials and methods

2.1 SF preparation

Bombyx mori silk cocoons were cut into small pieces and 5 g was then boiled at 80°C in 2 L of 0.02 M sodium carbonate (Na_2CO_3, Sigma-Aldrich) for 30 min with gentle stirring to disperse the silk fibres. The degummed SF was washed 3 times by stirring in distilled water for 20 min followed by replacing the water. The purified SF was squeezed well, stretched on a tray, and left overnight in a fume cupboard for the water to evaporate.

A solution of 10% wt/v degummed SF in non-aqueous medium was used for electrospinning. A solution of formic acid (FA, 98-100%, Fisher) and calcium chloride ($CaCl_2$, fused, granular, Fisher) with the ratio of 98 mL FA to 2 g $CaCl_2$ was prepared. The FA-$CaCl_2$ solution was used for the dissolution of SF (1 g of SF in 10 mL of FA-$CaCl_2$) by shaking with a vortex for a few minutes until the SF was completely dispersed in the solution, after which the SF solution was incubated at 45°C in a water bath overnight, and the solution turned dark pink in colour. The solution was filtered to get rid of debris that may block the electrospinning needle using a vacuum pump and a borosilicate glass filter (Pyrex®, porosity grade 1) prior to electrospinning.

2.2 Double layers electrospinning SF

The electrospinning solution (SF in FA/$CaCl_2$) was transferred to a 10 mL plastic syringe (BD Plastipak) with a flattened 19 G needle (BD Plastipak). It was then placed in a vertical electrospinning setup within an environmentally controlled chamber to fabricate the base layer of randomly aligned fibres. The tip of needle was placed 12 cm above the edge of the rotating mandrel with a width and diameter of 5 cm and 12 cm, respectively. Greaseproof paper (5 x 38 cm^2) was used as a collector and was wrapped around the width of the mandrel. The syringe was operated

at 0.4 mL/h constantly for 8 h by a syringe pump (Cole-Parmer). Meanwhile, the high voltage of 35 kV generated by DC voltage supplies was applied to the system (+30 kV at the needle and -5 kV at the rotating mandrel). The rotating speed of the collector was 800 rpm (5.03 m/s linear speed). Relative humidity (R.H.) and temperature were controlled at 35% R.H. and 25°C all the time.

After that, the collector and the SF solution in a syringe were relocated and placed in a horizontal electrospinning setup with the high rotating speed collector in order to deposit a layer of aligned fibres on top of the base layer of randomly aligned fibres. The working distance and feed rate were 12 cm and 0.4 mL/h; however, the voltage supply was reduced to 15 kV (+15 kV at the needle and 0 kV at the collector) and the rotating speed of collector was increased to 1500 rpm (9.42 m/s linear speed), and run for 4 h, yielding electrospun bilayer mats with thicknesses of ca. 100 μm. The thickness of fibre mat was measured by using a micrometer (DML3032, Digital Micrometers Ltd). Finally, electrospun SF mats were immersed in 80% ethanol for 20 min to induce β-sheet formation.

2.3 IPN of PEDOT:PSS on electrospun SF

3,4-ethylenedioxythiophene (EDOT, Sigma-Aldrich) was dispersed at 0.5% w/v in an aqueous solution of initiators containing 0.98% w/v sodium persulfate ($Na_2S_2O_8$, Sigma-Aldrich), and 0.2% w/v iron (II) sulfate heptahydrate ($Fe_2SO_4 \cdot 7H_2O$, Sigma-Aldrich) [52]. The dopant polystyrene sulfonate (PSS, Sigma-Aldrich) was added to the EDOT dispersion with various molar ratios to EDOT monomer (α) from 1.3 to 3.3 (approximately 0.84 – 2.13% wt/v) to produce a homogenous solution. The post-treated electrospun SF mats were immediately immersed in the working solution and left for 72 h at room temperature for polymerization and IPN formation. Over the

course of the reaction the solution changed from yellow to dark blue. After 72 h, the dark blue IPN materials were washed twice and preserved in distilled water to avoid shrinkage.

2.4 FTIR and HAXPES

The secondary structure of the SF was characterized by attenuated total reflectance – Fourier transform infrared spectroscopy (ATR – FTIR). The FTIR spectra were recorded between 4000 – 400 cm^{-1}. The amide I band (1700 – 1600 cm^{-1}) was analysed and deconvoluted using Origin software (OriginLab, USA). Three main structures; β-sheet, random coil, turns and bends were observed, assigned according to Wilson et al., 2000 [53]. β-sheets were assigned between 1621 – 1629 cm^{-1} and 1671 – 1679 cm^{-1}, random coils between 1641 – 1649 cm^{-1}, turns and bends were assigned between 1658 – 1671 cm^{-1} and 1681 – 1696 cm^{-1}, respectively.

The quantity of sulfur (S) present in PEDOT:PSS was determined by hard X-ray photoelectron spectroscopy (HAXPES-lab, Scienta Omicron GmbH), which uses a Ga Kα X-ray source (9.25 keV, Excillum), where an increase in kinetic energy of the emitted photoelectrons leads to an increase in sampling depth compared to surface-sensitive XPS using X-rays at energies of 1-2 keV [54, 55]. This allows for the bulk-like composition to be measured, minimizing the influence of surface contamination. Samples were attached to Omicron sample plates using adhesive copper tape for measurements under ultra-high vacuum with a base pressure of 6×10^{-10} mbar. A charge neutralizing low energy electron gun (FS40A, PREVAC) was used to replenish the electron supply after photoexcitation. The EW4000 electron energy analyzer with an entrance slit width of 1.5 mm was used to measure survey spectra, using a pass energy of 500 eV with an energy resolution of ~2 eV, and core level spectra of the elements of interest (C 1s at 285 eV binding energy (BE), N 1s at 400 eV BE, O 1s at 530 eV BE, and S 1s at 2470 eV BE), measured with 200 eV pass energy

with an energy resolution of ~0.8 eV [56]. Atomic concentrations were obtained using calculated sensitivity factors for the core levels, as described in [57] using recently published photoionization parameters up to 10 keV [58, 59]. The sampling depth, defined as $3\lambda \cos\theta$, where λ is the inelastic mean free path of electrons and θ is the electron take-off angle with respect to the surface normal [60], was calculated to be ~54 nm using the TPP-2M formula [61]. By tilting the sample and increasing the electron take-off angle, the sampling depth can be reduced towards the surface; θ was varied up to 70° to reduce the sampling depth to ~18 nm, and with combined Al Kα (1486 eV) XPS reduced the sampling depth to ~11 nm. Data were analyzed using CasaXPS [62].

2.5 Electrochemical characterisation

Cyclic voltammetry (CV) measurements were performed using a PalmSens EmStat 3+ potentiostat connected to a personal computer using the PSTrace 7.4 software, whereas electrochemical impedance spectroscopy (EIS) measurements were performed using an Ivium-n-Stat Multichannel Electrochemical Analyzer. For CV and EIS measurements, a three-electrode system was used with an Ag/AgCl reference electrode (CH Instruments, Inc. Austin, TX, USA), a platinum wire counter electrode (Sigma Aldrich, Gillingham, UK), and a working electrode (electrospun SF and IPN mats were cut into rectangular pieces of 1 x 3 cm, attached to glass slide by carbon tape prior to use). The electrodes were in a buffer (4 mL of phosphate-buffered saline [PBS] at pH 7.4) that was degassed with N_2. For CV measurements, the potential was swept between −1.0 V and +1.0 V vs. the Ag/AgCl electrode at a scan rate of 0.05 Vs^{-1}. For EIS measurements, the PBS also contained 5 mM of $[Fe(CN_6)]^{3-/4-}$, and measurements were performed with an open-circuit potential of 230 mV, with an amplitude of applied potential perturbation of 10 mV in the frequency range of 0.1 – 105,000 Hz.

187 *2.6 Electrical conductivity*

188 The conductance of fibres were measured in accordance with protocol IPC-TM-650, number
189 2.5.17.2 described by the Institute for Interconnecting and Packaging Electronic Circuits. Fibres
190 supported on glass slides were examined by chronoamperometry using a Keithley 2612B source
191 meter (Tektronix, Beaverton, US). Chronoamperometric measurements were made with a two-
192 point probe system (copper alligator clips), by connecting counter and reference electrodes
193 together. Briefly, two thin strips of adhesive-backed copper tape (Ted Pella, Inc., Redding, CA)
194 were attached to the films, parallel to one another, separated by a distance of 0.5 cm. The
195 working and counter electrodes were clipped on the strips of copper tape, and the current
196 measured for 30 seconds during a potential step experiment at 10 V. The electrodes were moved
197 to different positions after each measurement, and the current passed was recorded at three
198 different positions. The conductivity (S/m) of the fibre was determined in accordance with
199 equations (Supplementary information, table S2).

200 *2.7 Tensile tests*

201 The ultimate tensile stress (MPa), strain at break, Young's modulus (MPa), and toughness (kJ/m^3)
202 were tested by wet-state, horizontal tensile under water (ElectroForce, Planar Biaxial, TA
203 Instruments). Electrospun SF and IPNs mats were cut into small rectangular pieces of 5 x 35 mm^2,
204 with the direction of fibre alignment parallel to the sample length. The thicknesses of samples were
205 measured by a micrometer (DML3032, Digital Micrometers Ltd). The initial length between
206 tensile grips was 25 mm (5 mm of both ends were clamped). One grip connected to a load cell of
207 22 N was dynamic end with the moving speed of 10 μm/s, while another grip was stationary end.

2.8 NG108-15 cell culture

NG108-15, mouse neuroblastoma x rat glioma hybrid cells, were cultured in Dulbecco's Modified Eagle Medium (DMEM, Sigma) with high glucose supplemented with 10% fetal bovine serum (FBS), 1X – HAT solution (Fisher), and 1% antibiotic as a growth medium. They were incubated at 37°C, 5% CO_2. The medium was refreshed every 2 days until the cell confluence reached 60 – 70%, it was changed to a differentiation medium, growth medium with 0.75 mM cyclic adenosine monophosphate (cAMP, Stratech).

2.9 Media-extracting assay

The cytotoxicity of the electrospun SF and IPNs materials were tested by extracting assay (conditioned medium). The materials were cut into pieces of 3 x 3 cm^2, and sterilized with 70% ethanol for 10 min and UV exposure for 15 min. The materials were incubated with 6 mL of the growth medium at 37°C for 24 h. The extracted medium was exposed to NG108-15 in the subconfluent state. The cell morphology was observed, a live/dead assay undertaken, and DNA concentration determined for 72 h after exposure.

2.10 In Silico Toxicity Screening

In silico toxicity screening was carried out using Derek Nexus (v. 6.0.1, Nexus: 2.2.2) and Sarah Nexus (Sarah Nexus: 3.0.0, Sarah Model: 2.0) supplied by Lhasa Limited, Leeds, UK. Simplified molecular-input line-entry system (SMILES) notations for species analyzed are: formic acid, [H]C(O)=O; sodium persulfate, S(OOS([O-])(=O)=O)(=O)(=O)[O-].[Na+].[Na+]; EDOT, C1=C2C(=CS1)OCCO2; PEDOT, O1CCOC=2C1=C(SC=2C)C; PSS, C1=CC(=CC=C1C(CC)C)S(=O)(=O)[O-].

2.11 Direct contact assay

NG108-15 were cultured directly on electrospun SF and IPNs substrates. These materials were cut and mounted on 12 x 12 cm^2 glass coverslips. Materials were sterilized with 70% ethanol for 10 min and UV exposure for 15 min. They were washed twice with Dulbecco's phosphate buffer saline (DPBS, Sigma) and then incubated with 5 µg/mL laminin at 37°C for 2 h. NG108-15 cultured in a T-75 flask were trypsinized and placed on sample with the seeding density of 5 x 10^3 cells/cm^2 and cultured for 7 days. The growth medium was refreshed every 2 days. For the neurite extension study, the growth medium was changed to the differentiation medium at day 2, and continuously refreshed every 2 days. The cell metabolic activity, DNA concentration, and neurite length extension were observed for 7 days.

2.12 Cell metabolic activity and DNA concentration assays

Metabolic activity and DNA concentration were performed via resazurin and dsDNA PicoGreen® assays. They were determined at day 1, 3, 5, and 7. Samples with NG108-15 were washed twice with DPBS followed by 1 h incubation at 37^o C with growth medium containing 12.5 µg/mL of resazurin sodium salt (Sigma-Aldrich). Next, 100 µL medium was collected and the fluorescence intensity was measured.

Either NG108-15 cells or fibres with NG108-15 cells were taken from glass coverslips and put in 1.5 mL microcentrifuge tubes. 500 µL 1X Tris-EDTA (TE) buffer were added into the tubes, repeated freeze-thaw process three times, and centrifuged. 100 µL supernatants were collected and mixed with 100 µL PicoGreen® working solution for measuring fluorescence intensity. The excitation/emission of 544/590 nm and 485/520 nm with a Microplate Reader (FLUOstar) were used for resazurin and PicoGreen® assays respectively.

2.13 Live/dead assay

Live/dead assay is only used to determine the toxicity of chemical residues from fibre mats in the media-extracting assay (conditioned medium). Qualitative analysis of cell viability was observed by fluorescent microscopy (Nikon Eclipse 50i) with 10X magnification. Calcein AM (Invitrogen) and ethidium homodimer (EthD-1, Invitrogen) were diluted in DPBS, their final concentrations were 2 µM and 4 µM, respectively. Cells were stained with this working solution for 10 min at 37°C. Live cells were observed as uniform green in cytoplasm, while dead cells were shown as bright red spots at nucleus. The excitation/emission 495/515 nm and 495/635 nm were used for live and dead cells, respectively.

2.14 Scanning electron microscopy (SEM)

Typically, the surface of electrospun SF, IPNs mats, and also the neurite length of NG108-15 on substrates were observed by SEM (TESCAN MIRA3 and TESCAN VEGA3). Samples of NG108-15 were fixed with 2.5% glutaraldehyde in PBS for 30 min at 4°C and washed twice with PBS. After that, they were sequentially dehydrated through the series of ethanol gradients; 50%, 70%, 90%, and 100% for 5 min/each. Lastly, hexamethydisilazane (HDMS) was added to samples and they were left in a fume cupboard for evaporation of the HMDS overnight. The dried samples were then prepared and sputtered with Au/Pd (5 nm thickness) using an automatic gold sputter coater (Quorum) followed by SEM observation.

The direction of aligned fibres was always rotated to the position of 90º (12 o'clock) following the Cartesian coordinating system. The images were saved and collected in the format of .tif file. The fibre diameter, neurite length, and neurite orientation were then analysed using ImageJ software. The polarscatter and polarhistogram of neurite lengths were plotted using Matlab software

(MATLAB R2020a). Additionally, the oval profile plugin was used for measurement of fibre alignment and the 2D FFT alignment was calculated following it was mentioned in Ayres et al., 2008 [63]. The angle positions of 0° – 180° were considered in this study.

2.15 Immunofluorescence staining

β-III tubulin, an element of microtubule commonly found in neurites, was stained and qualitatively observed with a confocal microscope (CQ1, Yokogawa). Samples were fixed with 4% paraformaldehyde for 15 min. They were washed twice with PBS and permeabilised by adding 500 µL of Q & P solution (0.5% Triton X-100 in 0.2 M glycine in PBS) on each sample for 5 min at room temperature. After that, samples were washed twice with PBS and blocked non-specific proteins by adding 300 µL 2% fish skin gelatin (FSG) for 30 min. The primary antibody, rabbit polyclonal to β-III tubulin, were diluted in 2% FSG and incubated with the sample at 4°C overnight. The sample were washed twice again prior to the secondary antibody staining. Goat anti-rabbit IgG H&L (Alexa Fluor® 488) and DAPI were diluted in 2% FSG, added onto samples, and then incubated for 2 h in the dark area. The stained samples should be washed twice again, mounted onto glass slides with a prolonged mounting agent.

2.16 Statistical analysis

Data collected from samples were analysed by GraphPad Prism 8 software. Electrospun SF without PEDOT:PSS was used as a control parameter. Two-way ANOVA (Tukey) with $p < 0.03$ were considered as statistically significant.

3. Results

3.1 Preparation of electrospun SF

Double layers electrospun SF mats have the thickness of ~100 μm after 12 h electrospinning. The average diameters of fibres of the top (aligned fibre) and base (randomly aligned fibre) layers were relatively similar, 188 ± 55 nm and 177 ± 48 nm respectively. Ethanol-treatment and PEDOT:PSS IPN formation have no statistically significant effect on the fibre diameters (Supplementary information, Figure S1). The distributions of fibre diameters are shown in Figure 1c. The 2D FFT alignment results show the significant difference between the top and base layers. The peak of 2D FFT alignment value of the top layer was 2.25 at the positions of 88° – 90°, while that of the bottom layer was 9 times lower, it was 0.25 at the positions of 82° – 91° as shown in Figure 1d.

The secondary structure of the silk-based materials are altered by ethanol treatment, as confirmed by the FTIR results shown in Figures 1e and 1f. The amide I peak of electrospun SF was shifted from the wavenumber of 1651 cm^{-1} to between 1625 and 1621 cm^{-1} (indicative of β-sheet formation). The deconvolution of the amide I band spectra also reveals that the total secondary protein structures of untreated electrospun SF contains 55% β-sheet. Almost all ethanol treatment conditions increased β-sheet formation up to 63 – 65% except the condition of 70% ethanol.

Bulk – sensitive HAXPES demonstrates that the IPN formation protocol is a more effective method to generate electroactive SF-based biomaterials than dip coating (Supplementary information, Figure S2). Both surface – sensitive XPS and bulk – sensitive HAXPES show that the relative percentage of Sulfur (%S) to all elements (C, O, N, and S) of IPNs mats are higher than that of electrospun SF as shown in Figure 2. The relative %S of IPNs mats at the surface (~11 nm) were significantly higher than the other depths (~19 – 54 nm). It was 3.1% at the surface and

decreased to 1.6% over bulk material for IPN (α = 2.3), while it was 2.8% at the surface and decreased to 1.3% over bulk material for IPN (α = 3.3). Moreover, the fitting of the peaks of S 2p and S 1s of XPS and HAXPES confirm the successful polymerisation of PEDOT:PSS on/in electrospun SF as shown in Figure 2c. Each S 2p chemical species was fit with a spin-orbit split doublet, whereas the S 1s singlet state requires one peak for each chemical species. The spectra show two chemical species associated with PEDOT (S 2p3/2 at ~164 eV, S 1s at ~2472 eV binding energy) and PSS (S 2p3/2 at ~168 eV, S 1s at ~2477 eV binding energy) [64-66]. The relative amount of PSS and PEDOT is quite similar at both sampling depths for IPN (α = 2.3). It was 73% PSS at 11 nm, 69% at 54 nm for IPN (α = 2.3) and it was 78% PSS at 11 nm, 62% at 54 nm for IPN (α = 3.3).

The chemical states of C, N, O and S were also measured using XPS and angle-resolved HAXPES (Supplementary information, Figures S3 – S6). These results show little change in the relative amounts of each chemical state (e.g. the amount of PSS and PEDOT) from the surface into the bulk, suggesting a good level of polymerization has been achieved and that the simple IPN formation protocol yields a homogenous material (similar to reports of IPN generation in silk fibroin films [67], but in contrast to reports of IPN generation using silk fibroin materials that required two rounds of IPN formation to yield homogenous IPNs [11, 30]). The C 1s spectra indicate some excess hydrocarbon at the surface, and the N 1s spectra suggest some protonation at the surface, as is expected.

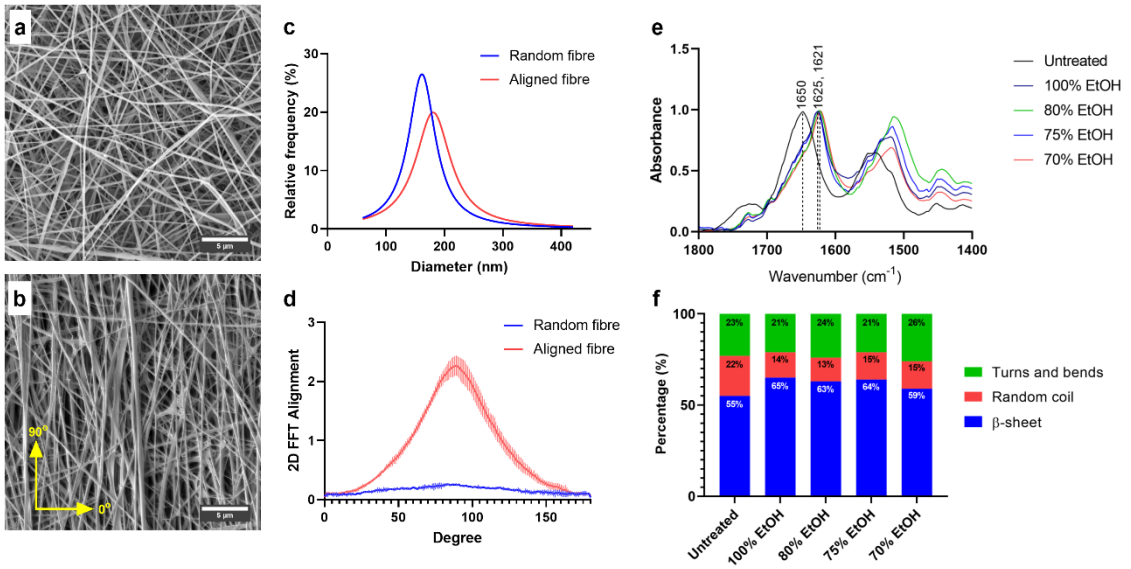

333

334 *Figure 1 Characterisation of double layer electrospun silk fibroin mats: (a) and (b) SEM of random and aligned fibres*
335 *SF with the scale bar of 5 µm and the orientation of 90º following the Cartesian coordinate system, (c) distribution of*
336 *fibre diameters, (d) 2D FFT alignment of fibres measured from 3 samples (3 independent electrospinning*
337 *experiments), (e) ATR-FTIR spectra of amide I band (1700 – 1600 cm^{-1}), and (f) the relative percentages of secondary*
338 *protein structures of electrospun SF after ethanol treatment.*

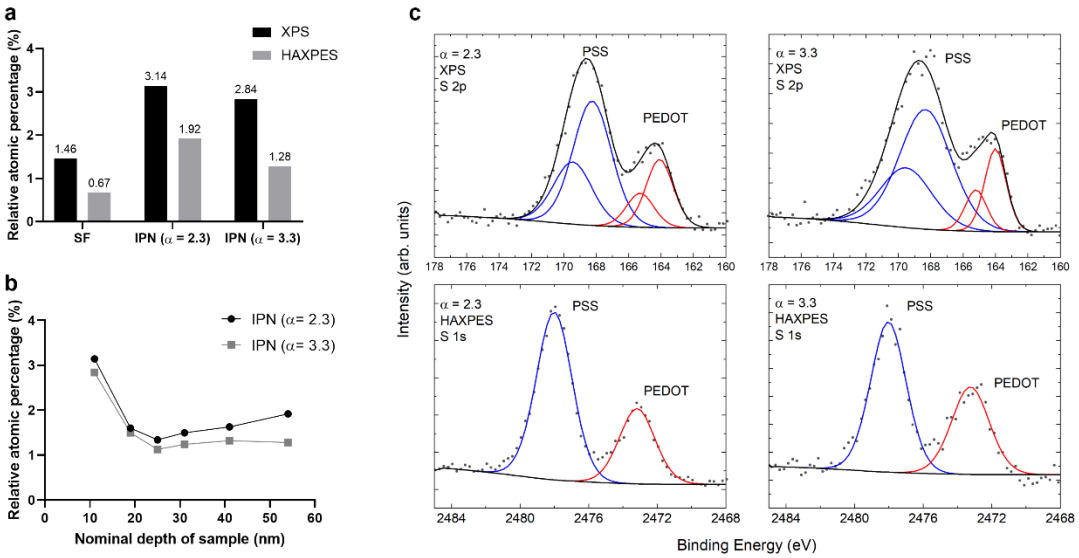

339

340 *Figure 2 surface-sensitive XPS and bulk-sensitive HAXPES analysis of electrospun SF, IPN (α = 2.3), and IPN (α =*
341 *3.3): (a) relative percentage of S compared to total elements (C,O, and N), (b) relative percentage of S of IPN mats*
342 *at different depths of sample, and (c) comparison of XPS and HAXPES spectra for S in the IPN mats. The S 2p and S*
343 *1s core levels are used for XPS and HAXPES measurements respectively, with sampling depths of ~11 and 54 nm.*

3.2 Electrical properties of electrospun SF and IPNs

The electrochemical properties of the materials were studied via cyclic voltammetry (CV) and electrical impedance spectroscopy (EIS), shown in Figure 3. CV was used to study the reduction/oxidation processes and electron-transfer properties of the IPNs; voltammograms of the materials show an anodic peak at ca. -0.2 V and the corresponding cathodic peak at ca. -0.6 V vs a Ag/AgCl reference electrode analogous to the literature [68] the somewhat unsymmetrical cathodic/anodic peaks are likely to be due to differences in background current and kinetic limitations [69, 70]. The Nyquist plots derived from EIS also showed semicircle curves in the high-frequency range due to electron-transfer resistance (R_{et}) of the materials, calculated by the difference of the real axis of impedance [71], and the vertical line that follows along the imaginary axis corresponds to a diffusion process. The R_{et} of IPN ($\alpha = 2.3$) and IPN ($\alpha = 3.3$) were ca. 330 Ω and 350 Ω, respectively suggesting the homogeneous coating of the materials with PEDOT:PSS. The electrical conductivity of pristine SF was ca. $\times 10^{-8}$ S/m, while those of IPN materials were ca. $\times 10^{-4}$ to 10^{-3} S/m (Supplementary information, table S2).

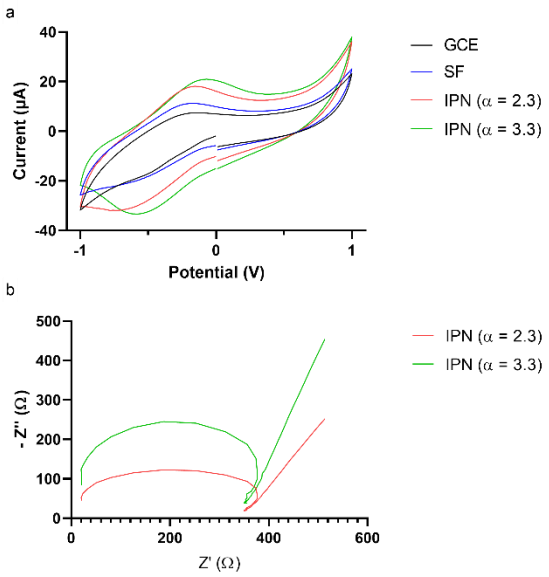

358

359 *Figure 3 Electrochemical characterisation of electrospun SF and IPN materials: (a) cyclic voltammetry (CV) data*
360 *and (b) Nyquist plots derived from electrochemical impedance spectroscopy (EIS).*

3.3 Mechanical properties of electrospun SF and IPNs materials

Electrospun SF mats are very fragile when they are dry. The ultimate tensile stress was 1.41 ± 0.21 MPa, the strain at break was 3 ± 1%, Young's modulus was 43.3 ± 16.8 MPa, and toughness was 12.7 ± 1.47 kJ/m^3. After ethanol treatment, the ultimate tensile stress was significantly increased to 2.62 ± 0.49 MPa but the strain was similar resulting in the higher Young's modulus as shown in the Figure 4. However, it is noteworthy that the mechanical properties of the electrospun SF are completely changed when the materials are soaked in water overnight, after which, the ultimate tensile stress was decreased to 0.87 ± 0.26 MPa while the strain was increased to 12 ± 2% indicating that these materials are more flexible in the wet state. For the IPNs (α = 2.3 and 3.3) mats in the wet state their stresses, strains, and toughness are slightly decreased from the wet state electrospun SF.

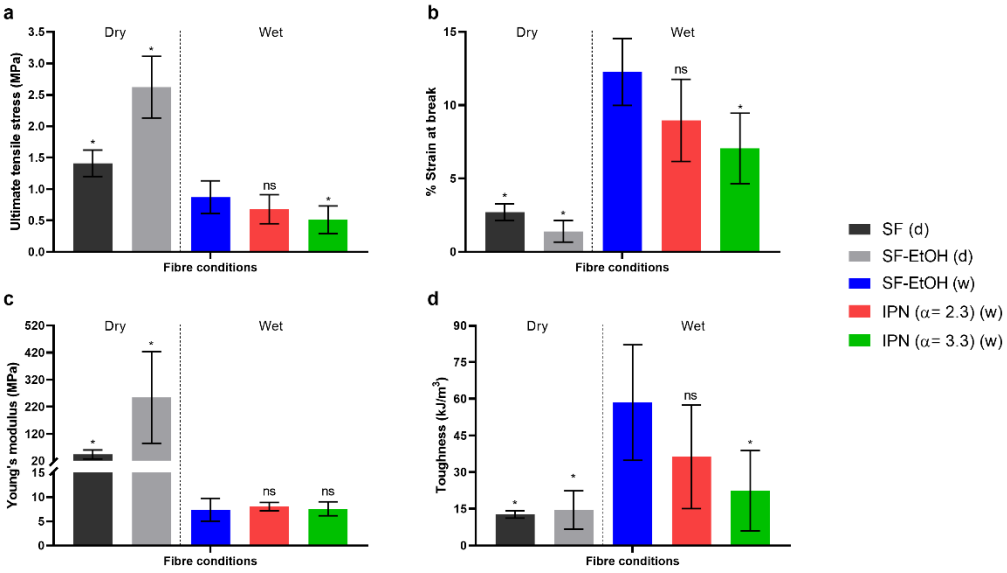

*Figure 4 Mechanical properties of electrospun SF and IPN mats in dry and wet states: (a) ultimate tensile stress, (b) % strain at break, (c) Young's modulus, and (d) toughness. All plotted with mean and SD. * represents the significant difference from the wet state ethanol-treated electrospun SF (Blue group), tested by One-Way ANOVA (Dunnett) with P-value ≤ 0.01. The n number represents the number of samples from three independent electrospinning experiments: SF (d) – (n = 3), SF-EtOH (d) – (n = 3), SF-ETOH (w) – (n = 9), IPN (α = 2.3) (w) – (n = 9), and IPN (α = 3.3) (w) – (n = 8).*

3.4 In silico toxicity and in vitro cytotoxicity studies

The safety data sheets for the starting materials and products (PEDOT-PSS for the dip-coating method; or EDOT, PSS, sodium persulfate and iron (II) sulfate heptahydrate for the IPN method) show PSS and PEDOT-PSS to be non-hazardous (according to Regulation (EC) No. 1272/2008), EDOT to be a toxic irritant, sodium persulfate to be a toxic sensitizer, and iron (II) sulfate heptahydrate to be a toxic irritant, highlighting the importance of effective washing prior to contemplating any biomedical applications. *In silico* toxicity screening of the various components was carried out using Derek Nexus [72] Derek Nexus: v. 6.0.1, Nexus: 2.2.2) and Sarah Nexus [73] (Sarah Nexus: v. 3.0.0, Sarah Model: 2.0) that can be used to assess the potential biocompatibility of materials (Derek identifies structural alerts for several endpoints and Sarah is a statistical-based model focused on mutagenicity only).[74-76] *In silico* toxicity screening studies showed PEDOT, PSS and PEDOT-PSS were non-sensitizers and non-mutagenic; however, formic acid was identified as an irritant by Derek Nexus, EDOT was identified as plausibly hepatotoxic by Derek Nexus, and sodium persulfate was identified as a plausible respiratory/skin sensitizer by Derek Nexus, reinforcing the importance of effective washing prior to contemplating any biomedical applications.

The pH of the extracted cell culture medium of electrospun SF and IPNs (α = 2.3 and 3.3) was approximately 7.8, similar to the normal growth medium, demonstrating no residual acidic components leaching from the materials (and importantly, the efficiency of the sample preparation). Subconfluent NG108-15 cells on glass substrates exposed to these extracted media can grow and proliferate slowly, confirmed by the DNA concentration result as shown in Figure 5a. Importantly, the DNA concentrations of NG108-15 after exposure to extracted media gradually increased over time, although they were slightly lower than the control condition, NG108-15

cultured on tissue culture plastic (TCP) with the normal growth medium; these subtle differences in the first few days are accounted for by surface chemistry and time taken for the cells to produce their own extracellular matrices.

The live/dead staining reveals that the cell morphology is slightly changed after exposure by the extracted media. Live cells and dead cells are stained in green and red respectively as shown in Figure 5b – e. Commonly, NG108-15 grow individually and evenly spread all over the area. Each cell can extend small neurites from its cell body. There are more clusters of rounded cells once cultured with extracted media especially from IPN conditions as shown in the Figure 5d and 5e.

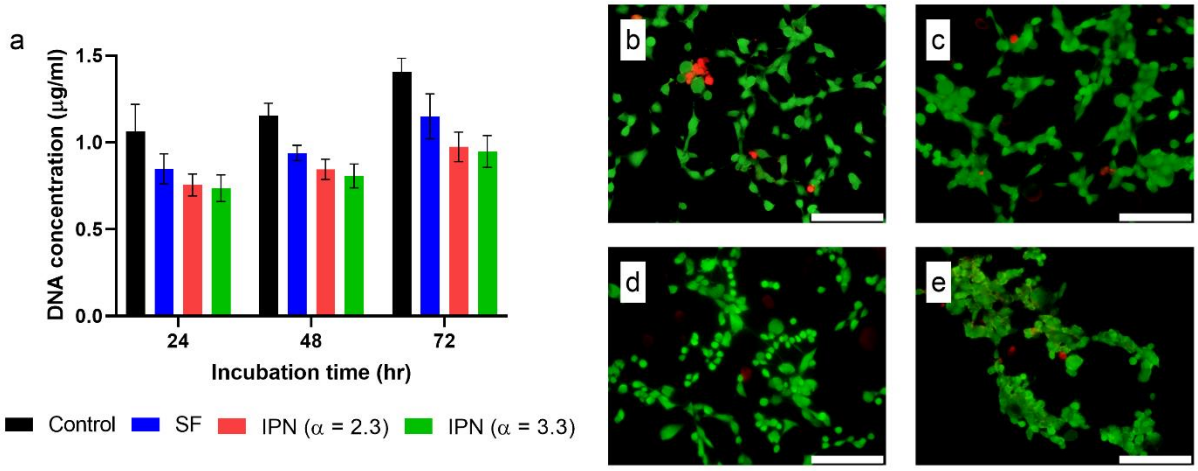

Figure 5 NG108-15 grown on TCP with the extracted media (conditioned media): (a) DNA concentration of NG108-15 cultured in normal growth medium, extracted medium of electrospun SF and IPNs (α = 2.3 and 3.3) for 24 – 72 hr, (n=3) no significant different between SF and IPNs groups. The live/dead staining of NG 108-15 on glass substrates after incubated with (b) normal growth medium, (c) extracted medium of electrospun SF, (d) extracted medium of IPN (α = 2.3), and (e) extracted medium of IPN (α = 3.3) at 72 hr with the scale bar of 150 µm.

3.5 neuron growth, neurite extension and orientation

In accordance with results of the media-extraction assay, live/dead staining suggested that the electrospun SF and IPNs mats were biocompatible without toxicity from any chemical residue eluting from the IPNs. In the direct contact assay, NG108-15 grown on electrospun SF and IPNs mats were examined by the metabolic activity and DNA concentration. Previous studies showed that metabolic activity correlated with cell viability [48, 49]; thus, it was used in the direct test instead of the live/dead staining, and the morphology of cells on fibres was observed using SEM and immunofluorescence.

The metabolic activity and DNA concentration profiles of NG108-15 directly cultured on uncoated substrates and laminin coated substrates are similar (Figure 6). Typically, the metabolic activity was observed to increase from ~50 to 1200 A.U., and the DNA concentration was observed to increase from ~0.1 to 0.5 µg/mL over the period of 7 days. The metabolic activity of the electrospun SF condition was significantly higher than that of IPN ($\alpha = 3.3$) at day 5, but similar at day 7. Additionally, the DNA concentration of the electrospun SF condition was higher than that of IPN ($\alpha = 2.3$ and 3.3) at day 3 and 5, while they are similar at day 7 as well.

Furthermore, SEM results support the observation that NG108-15 can grow and extend their neurites on electrospun SF and IPNs materials for 7 days, even though they were cultured without the differentiation factor, cAMP. We observe that neurite extension lengths on the laminin coated materials are slightly longer than on uncoated materials (Supplementary information, Figure S7). Although the average neurite lengths are similar (around 30 – 40 µm) for all conditions and substrates, the 90^{th} percentiles of the neurite lengths are different. Neurite lengths are 55, 45, and

50 µm on laminin coated electrospun SF, IPN ($\alpha = 2.3$), and IPN ($\alpha = 3.3$), while, they are 35, 50, and 40 µm on uncoated electrospun SF, IPN ($\alpha = 2.3$), and IPN ($\alpha = 3.3$), respectively.

In the differentiation phase of NG108-15, cells are grown as clusters and extend many more longer neurites compared to the normal growth phase as shown in Figure 7. The immunofluorescence confirms the processes extended from the cell clusters are neurites due to the β-III tubulin staining. The average neurite length in this phase is ~80 µm for all conditions. Interestingly, most neurites are orientated in the parallel direction to the fibre alignment (evidence of the instructive nature of the topological cues imparted by fibre alignment), which is in the position of 90^{o} in the polar-plots of Figure 8. The maximum neurite lengths reach to 300 µm in the condition of laminin coated electrospun SF and laminin coated IPN ($\alpha = 2.3$). The other conditions have the maximum neurite length of ~200 – 250 µm. The 90^{th} percentiles of the neurite length are ~120 – 140 µm in all condition except laminin coated electrospun SF, which is 180 µm.

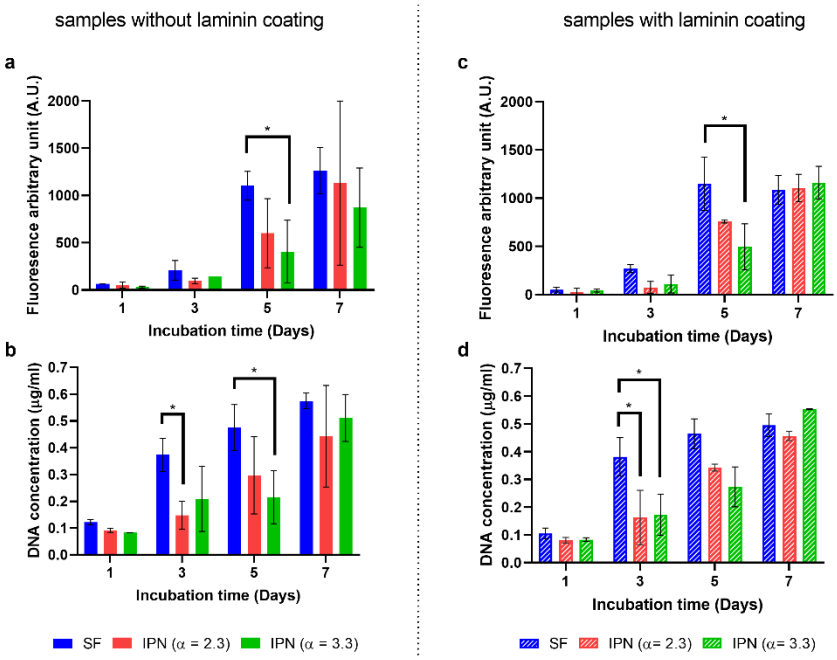

449

450 *Figure 6 <u>In vitro</u> biocompatibility results of NG108-15 directly cultured on electrospun SF and IPNs mats for 7 days:*
451 *(a) cell metabolic activity and (b) DNA concentration of uncoated substrates. (c) cell metabolic activity and (d) DNA*
452 *concentration of laminin-coated substrates, * represents the significant difference via Tukey's multiple comparisons*
453 *test comparing to SF as a control with P value ≤ 0.03, (n = 3 independent samples).*

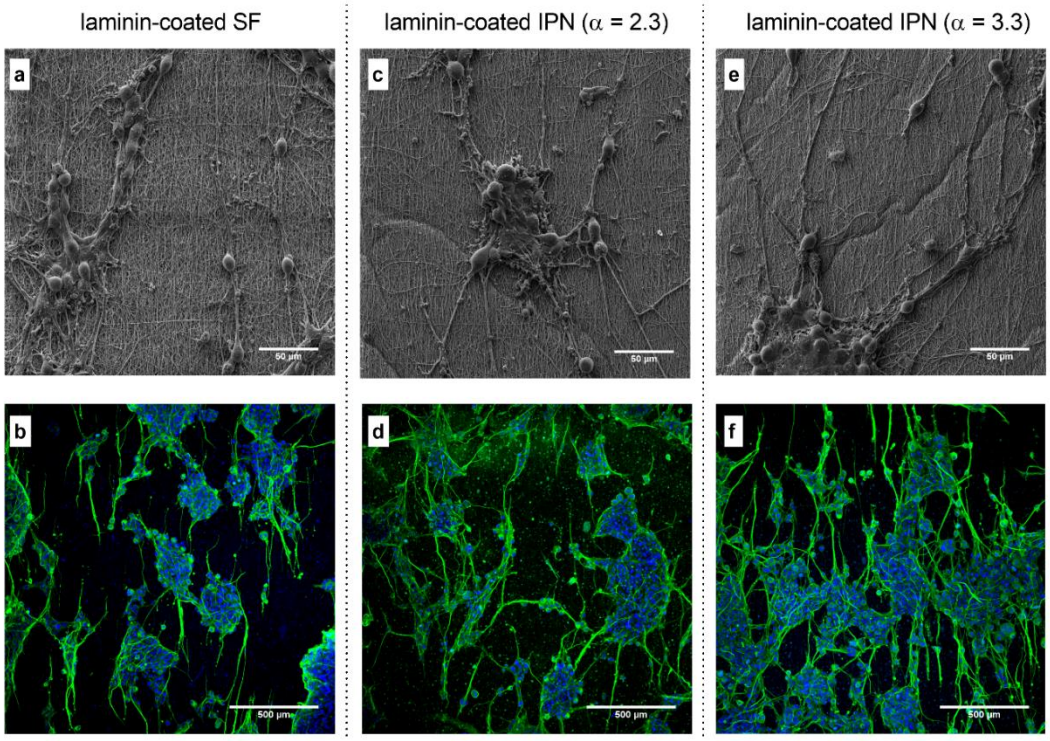

Figure 7 SEM and immunofluorescence staining of differentiated NG108-15 on laminin coated electrospun SF and IPNs mats. The alignment of fibres is at 90º following the Cartesian coordinate system. The nuclei are stained with DAPI (blue) and the β-III tubulin representing neurites are stained with Alexa Fluor® 488 (green).

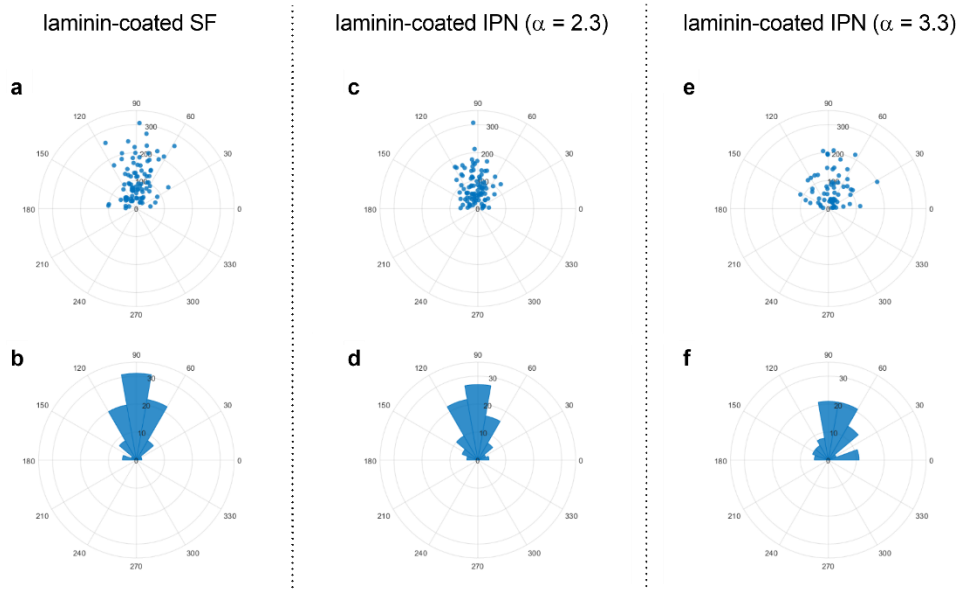

Figure 8 Neurite orientation and length of differentiated NG108-15 on laminin-coated electrospun SF and IPNs mats at day 7: (a, c, and d) the polarscatters of neurites oriented in the different angles, the radius represents the length of neurite (µm). (b, d, and f) the polarhistogram of neurites, the radius represents the relative percentage of number of neurites aligned in the different angles from 0º – 180º with the bin width of 20°.

4. Discussion

4.1 Novel method for electrospinning SF and PEDOT:PSS modification

Commonly, the preparation of SF from silk cocoons requires 4 sequential steps: degumming, dissolution, dialysis, and either lyophilisation followed by more processing [18] or film casting followed by more processing [77, 78]. There are two well known protocols using aqueous solvents, LiBr solution [18] and $CaCl_2$/ethanol/water [79] to dissolve the degummed SF, both of which disrupt the β-sheets present in the silk fibroin fibres within a few hours, and require dialysis thereafter. Dialysis is time-consuming and potentially complicated by gelation during dialysis, and to avoid these complications we prepared the electrospinning SF solution via a dialysis free protocol using a non-aqueous solvent system.

SF can be processed in various non-aqueous solvent systems, including FA [78, 80-82], hexafluoroisopropanol (HFIP) [83], dichloromethane (DCM) [84], etc.; FA with the addition of $CaCl_2$ can dissolve degummed SF within 3 h, enabling film casting and subsequent re-dissolution for electrospinning later [85]. This led to the idea of preparing electrospinning SF without the casting/redissolution in FA/$CaCl_2$, yielding fibres with diameters of ~200 nm.

The electrospun SF can be rendered conductive either via dip coating or via growth of an IPN of PEDOT:PSS in/on the electrospun SF, as assessed visually (by color change from off white to blue) and confirmed by HAXPES (showing higher %S especially at the surface of material, ~11 nm). The S1 s spectra show the same ratio between PSS and PEDOT peaks at all depths of the IPNs. The higher S content of IPNs than on dip coated materials is likely due to the non-covalent adsorption of PEDOT:PSS on SF during dip coating is significantly weaker than the covalent bonds formed during IPN formation between the EDOT and aromatic amino acids on SF.

4.2 Flexibility and electrical conductivity of electrospun SF

The formation of β-sheets in the electrospun SF after ethanol treatment increases the mechanical properties. In the wet state, the electrospun materials are more flexible than in the dry state due to the plasticization of the SF chains by water [86]. The IPNs are all somewhat weaker than the electrospun SF alone which is likely to be due to disruption of hydrogen bonding between the protein chains after growth of the IPN.

The electrical conductivity of the SF/PEDOT:PSS IPN materials (ca. 10^{-4} to 10^{-3} S/m) shows they are semiconductors (similar to the literature [26, 87]), while the pristine SF is an insulator [24-26]. In a previous study of our groups, the conductivity of SF/PEDOT:PSS prepared via another coating technique was also in the range of semiconductors ($\times10^{-3}$ to 10^{1} S/m), influenced by the concentration of PEDOT:PSS [48], which highlights the effects of subtly different processing on the properties of the electroactive biomaterials.

4.3 Effects of PEDOT:PSS on the neural growth

PEDOT:PSS can promote neurogenic differentiation and the expression of β-III tubulin in neurites [38]. The in silico toxicity study suggests any residues from the preparation and processing of electrospun SF and IPNs may hinder cell growth, however, thorough washing minimized such complications. In vitro studies using NG108-15 cells indicate their aggregation as clusters without high levels of dead cells once cultured with the extracted medium of IPNs mats, pH = 7.8. Interestingly, more cell clusters were observed on the conductive IPNs than the non-conductive electrospun SF regardless of whether they were coated with laminin or not, suggesting subtle differences in cell-material interactions are important for cell differentiation; [88] and that cell

aggregates were also observed when NG108-15 cells were cultured with the differentiation medium as well (Supplementary information, S8).

4.4 Neurites extension and orientation on sub-micron aligned fibres

A previous study using analogous nanofibrous SF/PEDOT:PSS-based biomaterials were shown to adsorb more protein (Bovine serum albumin) than pristine SF [48], and proteins such as gelatin have been used to render PEDOT-based biomaterials more cell adhesive [89]. In this study the IPNs were coated with a thin layer of adsorbed laminin (akin to other studies where laminin was used to coat electrodes for cell culture with small changes to impedance [90] and no significant changes in the electrochemical properties of the electrodes [91]), however, quantification of laminin adsorbtion on such complex hydrophilic nanofibrous IPNs is not reproducibly measurable. The laminin-coating of all substrates was used to enhance cell adhesion and promote the neurite length. There is a small increase of neurite length ~10 μm on laminin-coated substrates but no significant difference between electrospun SF and the IPNs. These results suggest that the conductive IPN biomaterials induce cell aggregation which is involved in cell differentiation [88].

In the differentiation phase, a cluster of cells extends neurites with increased lengths compared to the growth phase. Most neurites are oriented parallel to the fibre alignment of electrospun SF, confirming the sub-micron aligned electrospun SF can control the direction of neurite extension. Moreover, the laminin-coated substrates promote longer neurites. The average length of neurite on laminin-coated electrospun SF and IPNs are similar; however, it is noteworthy that the longest neurite outgrowth of 300 μm was observed in the parallel direction of fibre alignment on laminin-coated electrospun SF and IPN ($\alpha = 2.3$) mats, which is also the material with the lowest electron

transfer resistance (R_{et}, ca. 330 Ω). This suggests that PEDOT:PSS is a supportive factor for neural differentiation but it has no crucial effects on neurite outgrowth compared to cAMP and laminin.

5. Conclusion

This novel fabrication method of double layer electrospinning SF can produce sub-micron fibres with aligned fibres to direct axon orientation. The electrospun SF material is brittle in the dry state and more flexible in the wet state due to water plasticization. Once coated with laminin, both electrospun SF and IPN materials promote the similar length of neurite extension. These developed materials, IPN of PEDOT:PSS on/in electrospun SF is novel, potentially enabling electrical stimulation of the cells and facilitating peripheral nerve regeneration.

6. Acknowledgements

This work was supported by the Henry Royce Institute for Advanced Materials, funded through EPSRC grants EP/R00661X/1, EP/P025021/1 and EP/P025498/1. We thank Zara L. Smith at University of Manchester for assistance with immunofluorescence staining, Garry R. Harper and Vasileios K. Oikonomou at Lancaster University for assistance with early attempts at silk processing. We also thank the Royal Thai Government Scholarship for support of C.P., the EPSRC (EP/R512564/1, 2065445) for support of M.D.A. and J.G.H., the BBSRC (grant BB/L0137971/1) for support of G.R.H. and J.G.H., and the British Council of Greece for the IELTS Award 2017 for support of V.K.O.

7. References

[1] K. Haastert-Talini, C. Grothe, Electrical Stimulation for Promoting Peripheral Nerve Regeneration, International Review of Neurobiology, Elsevier Inc.2013, pp. 111-124.

[2] R.M. Meadows, D.R. Sengelaub, K.J. Jones, Chapter 29 - Cellular Aspects of Nerve Injury and Regeneration A2 - Tubbs, R. Shane, in: E. Rizk, M.M. Shoja, M. Loukas, N. Barbaro, R.J. Spinner (Eds.), Nerves and Nerve Injuries, Academic Press, San Diego, 2015, pp. 433-449.

[3] A. Faroni, S.A. Mobasseri, P.J. Kingham, A.J. Reid, Peripheral nerve regeneration: experimental strategies and future perspectives, Adv Drug Deliv Rev 82-83 (2015) 160-7.

[4] R. Zhang, J.M. Rosen, The role of undifferentiated adipose-derived stem cells in peripheral nerve repair, Neural Regen Res 13(5) (2018) 757-763.

[5] Y. Sowa, T. Kishida, T. Imura, T. Numajiri, K. Nishino, Y. Tabata, O. Mazda, Adipose-Derived Stem Cells Promote Peripheral Nerve Regeneration In Vivo without Differentiation into Schwann-Like Lineage, Plast Reconstr Surg 137(2) (2016) 318e-330e.

[6] A.N. Leberfinger, D.J. Ravnic, R. Payne, E. Rizk, S.V. Koduru, S.W. Hazard, Adipose-Derived Stem Cells in Peripheral Nerve Regeneration, Curr Surg Rep 5(2) (2017).

[7] K. Haastert-Talini, C. Grothe, Chapter Five - Electrical Stimulation for Promoting Peripheral Nerve Regeneration, in: S. Geuna, I. Perroteau, P. Tos, B. Battiston (Eds.), International Review of Neurobiology, Academic Press2013, pp. 111-124.

[8] Y.S. Chen, C.L. Hu, C.L. Hsieh, J.G. Lin, C.C. Tsai, T.H. Chen, C.H. Yao, Effects of percutaneous electrical stimulation on peripheral nerve regeneration using silicone rubber chambers, J Biomed Mater Res 57(4) (2001) 541-549.

[9] C.H. Yao, R.L. Chang, S.L. Chang, C.C. Tsai, F.J. Tsai, Y.S. Chen, Electrical stimulation improves peripheral nerve regeneration in streptozotocin-induced diabetic rats, J Trauma Acute Care 72(1) (2012) 199-205.

[10] J.H. Huang, L. Lu, X.Y. Hu, Z.X. Ye, Y. Peng, X.D. Yan, D. Geng, Z.J. Luo, Electrical Stimulation Accelerates Motor Functional Recovery in the Rat Model of 15-mm Sciatic Nerve Gap Bridged by Scaffolds With Longitudinally Oriented Microchannels, Neurorehab Neural Re 24(8) (2010) 736-745.

[11] J.G. Hardy, Z.Z. Khaing, S.J. Xin, L.W. Tien, C.E. Ghezzi, D.J. Mouser, R.C. Sukhavasi, R.C. Preda, E.S. Gil, D.L. Kaplan, C.E. Schmidt, Into the groove: instructive silk-polypyrrole films with topographical guidance cues direct DRG neurite outgrowth, J Biomat Sci-Polym E 26(17) (2015) 1327-1342.

[12] S. Das, M. Sharma, D. Saharia, K.K. Sarma, E.M. Muir, U. Bora, Electrospun silk-polyaniline conduits for functional nerve regeneration in rat sciatic nerve injury model, Biomed Mater 12(4) (2017).

[13] J.Y. Lee, C.A. Bashur, A.S. Goldstein, C.E. Schmidt, Polypyrrole-coated electrospun PLGA nanofibers for neural tissue applications, Biomaterials 30(26) (2009) 4325-35.

[14] M.P. Prabhakaran, L. Ghasemi-Mobarakeh, G.R. Jin, S. Ramakrishna, Electrospun conducting polymer nanofibers and electrical stimulation of nerve stem cells, J Biosci Bioeng 112(5) (2011) 501-507.

[15] J.G. Hardy, R.C. Cornelison, R.C. Sukhavasi, R.J. Saballos, P. Vu, D.L. Kaplan, C.E. Schmidt, Electroactive Tissue Scaffolds with Aligned Pores as Instructive Platforms for Biomimetic Tissue Engineering, Bioengineering-Basel 2(1) (2015) 15-34.

[16] A. Magaz, A.D. Roberts, S. Faraji, T.R.L. Nascimento, E.S. Medeiros, W.Z. Zhang, R.D. Greenhalgh, A. Mautner, X. Li, J.J. Blaker, Porous, Aligned, and Biomimetic Fibers of Regenerated Silk Fibroin Produced by Solution Blow Spinning, Biomacromolecules 19(12) (2018) 4542-4553.

[17] A. Magaz, A. Faroni, J.E. Gough, A.J. Reid, X. Li, J.J. Blaker, Bioactive Silk-Based Nerve Guidance Conduits for Augmenting Peripheral Nerve Repair, Adv Healthc Mater 7(23) (2018).

[18] D.N. Rockwood, R.C. Preda, T. Yucel, X.Q. Wang, M.L. Lovett, D.L. Kaplan, Materials fabrication from Bombyx mori silk fibroin, Nat Protoc 6(10) (2011) 1612-1631.

[19] C.Z. Zhou, F. Confalonieri, M. Jacquet, R. Perasso, Z.G. Li, J. Janin, Silk fibroin: Structural implications of a remarkable amino acid sequence, Proteins 44(2) (2001) 119-122.
[20] G.H. Altman, F. Diaz, C. Jakuba, T. Calabro, R.L. Horan, J.S. Chen, H. Lu, J. Richmond, D.L. Kaplan, Silk-based biomaterials, Biomaterials 24(3) (2003) 401-416.
[21] B. Kundu, R. Rajkhowa, S.C. Kundu, X.G. Wang, Silk fibroin biomaterials for tissue regenerations, Adv Drug Deliver Rev 65(4) (2013) 457-470.
[22] M. Dodel, N.H. Nejad, S.H. Bahrami, M. Soleimani, L.M. Amirabad, H. Hanaee-Ahvaz, A. Atashi, Electrical stimulation of somatic human stem cells mediated by composite containing conductive nanofibers for ligament regeneration, Biologicals 46 (2017) 99-107.
[23] S. Aznar-Cervantes, J.G. Martinez, A. Bernabeu-Esclapez, A.A. Lozano-Perez, L. Meseguer-Olmo, T.F. Otero, J.L. Cenis, Fabrication of electrospun silk fibroin scaffolds coated with graphene oxide and reduced graphene for applications in biomedicine, Bioelectrochemistry 108 (2016) 36-45.
[24] C. Jang, j.k. Park, G.-H. Yun, H.H. Choi, H.-J. Lee, J.-G. Yook, Radio-Frequency/Microwave Gas Sensors Using Conducting Polymer, Materials 13 (2020) 2859.
[25] T.-H. Le, Y. Kim, H. Yoon, Electrical and Electrochemical Properties of Conducting Polymers, Polymers 9 (2017) 150.
[26] G. Kaur, R. Adhikari, P. Cass, M. Bown, P. Gunatillake, Electrically conductive polymers and composites for biomedical applications, RSC Advances 5(47) (2015) 37553-37567.
[27] R. Yadav, R. Purwar, Influence of metal oxide nanoparticles on morphological, structural, rheological and conductive properties of mulberry silk fibroin nanocomposite solutions, Polymer Testing 93 (2021) 106916.
[28] Q. Sun, B. Qian, K. Uto, J. Chen, X. Liu, T. Minari, Functional biomaterials towards flexible electronics and sensors, Biosensors and Bioelectronics 119 (2018) 237-251.
[29] R. Ranjana, N. Parushuram, K.S. Harisha, S. Asha, B. Narayana, M. Mahendra, Y. Sangappa, Fabrication and characterization of conductive silk fibroin–gold nanocomposite films, Journal of Materials Science: Materials in Electronics 31(1) (2020) 249-264.
[30] J.G. Hardy, S.A. Geissler, D. Aguilar, M.K. Villancio-Wolter, D.J. Mouser, R.C. Sukhavasi, R.C. Cornelison, L.W. Tien, R.C. Preda, R.S. Hayden, J.K. Chow, L. Nguy, D.L. Kaplan, C.E. Schmidt, Instructive Conductive 3D Silk Foam-Based Bone Tissue Scaffolds Enable Electrical Stimulation of Stem Cells for Enhanced Osteogenic Differentiation, Macromol Biosci 15(11) (2015) 1490-1496.
[31] B.B. Sun, T. Wu, J. Wang, D.W. Li, J. Wang, Q. Gao, M.A. Bhutto, H. El-Hamshary, S.S. Al-Deyab, X.M. Mo, Polypyrrole-coated poly(L-lactic acid-co-epsilon-caprolactone)/silk fibroin nanofibrous membranes promoting neural cell proliferation and differentiation with electrical stimulation, J Mater Chem B 4(41) (2016) 6670-6679.
[32] S. Aznar-Cervantes, A. Pagan, J.G. Martinez, A. Bernabeu-Esclapez, T.F. Otero, L. Meseguer-Olmo, J.I. Paredes, J.L. Cenis, Electrospun silk fibroin scaffolds coated with reduced graphene promote neurite outgrowth of PC-12 cells under electrical stimulation, Mat Sci Eng C-Mater 79 (2017) 315-325.
[33] S. Tsukada, H. Nakashima, K. Torimitsu, Conductive Polymer Combined Silk Fiber Bundle for Bioelectrical Signal Recording, Plos One 7(4) (2012).
[34] R.K. Pal, A.A. Farghaly, C.Z. Wang, M.M. Collinson, S.C. Kundu, V.K. Yadavalli, Conducting polymer-silk biocomposites for flexible and biodegradable electrochemical sensors, Biosens Bioelectron 81 (2016) 294-302.
[35] H.S. Park, S.J. Ko, J.S. Park, J.Y. Kim, H.K. Song, Redox-active charge carriers of conducting polymers as a tuner of conductivity and its potential window, Sci Rep-Uk 3 (2013).
[36] A.V. Volkov, K. Wijeratne, E. Mitraka, U. Ail, D. Zhao, K. Tybrandt, J.W. Andreasen, M. Berggren, X. Crispin, I.V. Zozoulenko, Understanding the Capacitance of PEDOT:PSS, Adv Funct Mater 27(28) (2017).

[37] M. Anderson, N.B. Shelke, O.S. Manoukian, X. Yu, L.D. McCullough, S.G. Kumbar, Peripheral Nerve Regeneration Strategies: Electrically Stimulating Polymer Based Nerve Growth Conduits, Crit Rev Biomed Eng 43(2-3) (2015) 131-59.
[38] S. Sirivisoot, R. Pareta, B.S. Harrison, Protocol and cell responses in three-dimensional conductive collagen gel scaffolds with conductive polymer nanofibres for tissue regeneration, Interface Focus 4(1) (2014).
[39] J.A. Sierra-Fonseca, O. Najera, J. Martinez-Jurado, E.M. Walker, A. Varela-Ramirez, A.M. Khan, M. Miranda, N.S. Lamango, S. Roychowdhury, Nerve growth factor induces neurite outgrowth of PC12 cells by promoting Gbetagamma-microtubule interaction, BMC Neurosci 15 (2014) 132.
[40] P. Moroder, M.B. Runge, H. Wang, T. Ruesink, L. Lu, R.J. Spinner, A.J. Windebank, M.J. Yaszemski, Material properties and electrical stimulation regimens of polycaprolactone fumarate-polypyrrole scaffolds as potential conductive nerve conduits, Acta Biomater 7(3) (2011) 944-53.
[41] H.T. Nguyen, S. Sapp, C. Wei, J.K. Chow, A. Nguyen, J. Coursen, S. Luebben, E. Chang, R. Ross, C.E. Schmidt, Electric field stimulation through a biodegradable polypyrrole-co-polycaprolactone substrate enhances neural cell growth, J Biomed Mater Res A 102(8) (2014) 2554-64.
[42] T. Fukazawa, M. Matsumoto, T. Imura, E. Khalesi, T. Kajiume, Y. Kawahara, K. Tanimoto, L. Yuge, Electrical stimulation accelerates neuromuscular junction formation through ADAM19/neuregulin/ErbB signaling in vitro, Neurosci Lett 545 (2013) 29-34.
[43] J.A. Doebler, Effects of neutral ionophores on membrane electrical characteristics of NG108-15 cells, Toxicol Lett 114(1-3) (2000) 27-38.
[44] J.A. Doebler, Effects of protonophores on membrane electrical characteristics in NG108-15 cells, Neurochem Res 25(2) (2000) 263-8.
[45] M.C. Acosta-García, I. Morales-Reyes, A. Jiménez-Anguiano, N. Batina, N.P. Castellanos, R. Godínez-Fernández, Simultaneous recording of electrical activity and the underlying ionic currents in NG108-15 cells cultured on gold substrate, Heliyon 4(2) (2018) e00550.
[46] M.K. Gheith, T.C. Pappas, A.V. Liopo, V.A. Sinani, B.S. Shim, M. Motamedi, J.P. Wicksted, N.A. Kotov, Stimulation of Neural Cells by Lateral Currents in Conductive Layer-by-Layer Films of Single-Walled Carbon Nanotubes, Advanced Materials 18(22) (2006) 2975-2979.
[47] K. Pawar, G. Welzel, C. Haynl, S. Schuster, T. Scheibel, Recombinant Spider Silk and Collagen-Based Nerve Guidance Conduits Support Neuronal Cell Differentiation and Functionality in Vitro, ACS Applied Bio Materials 2(11) (2019) 4872-4880.
[48] A. Magaz, B.F. Spencer, J.G. Hardy, X. Li, J.E. Gough, J.J. Blaker, Modulation of Neuronal Cell Affinity on PEDOT-PSS Nonwoven Silk Scaffolds for Neural Tissue Engineering, Acs Biomater Sci Eng 6(12) (2020) 6906-6916.
[49] A. Magaz, X. Li, J.E. Gough, J.J. Blaker, Graphene oxide and electroactive reduced graphene oxide-based composite fibrous scaffolds for engineering excitable nerve tissue, Mater Sci Eng C Mater Biol Appl 119 (2021) 111632.
[50] P.J. Kingham, D.F. Kalbermatten, D. Mahay, S.J. Armstrong, M. Wiberg, G. Terenghi, Adipose-derived stem cells differentiate into a Schwann cell phenotype and promote neurite outgrowth in vitro, Exp Neurol 207(2) (2007) 267-74.
[51] D. Kraus, V. Boyle, N. Leibig, G.B. Stark, V. Penna, The Neuro-spheroid—A novel 3D in vitro model for peripheral nerve regeneration, Journal of Neuroscience Methods 246 (2015) 97-105.
[52] T. Horii, H. Hikawa, M. Katsunuma, H. Okuzaki, Synthesis of highly conductive PEDOT:PSS and correlation with hierarchical structure, Polymer 140 (2018) 33-38.
[53] D. Wilson, R. Valluzzi, D. Kaplan, Conformational transitions in model silk peptides, Biophys J 78(5) (2000) 2690-2701.
[54] J.C. Woicik, Hard X-ray Photoelectron Spectroscopy (HAXPES) Preface, Springer Ser Surf Sc 59 (2016) V-Vi.

[55] G. Panaccione, K. Kobayashi, Hard X-ray photoemission spectroscopy: Variable depth analysis of bulk, surface and interface electronic properties, Surf Sci 606(3-4) (2012) 125-129.
[56] A. Regoutz, M. Mascheck, T. Wiell, S.K. Eriksson, C. Liljenberg, K. Tetzner, B.A.D. Williamson, D.O. Scanlon, P. Palmgren, A novel laboratory-based hard X-ray photoelectron spectroscopy system, Rev Sci Instrum 89(7) (2018).
[57] B.F. Spencer, S. Maniyarasu, B. Reed, D.J.H. Cant, R. Ahumada-Lazo, A.G. Thomas, C.A. Muryn, M. Maschek, S.K. Eriksson, T. Wiell, T.-L. Lee, S. Tougaard, S.G. Shard, W.R. Flavell, Hard X-rays and inelastic background modelling extend photoelectron spectroscopy below the surface for the detection of buried layers, Applied Surface Science (2020).
[58] M.B. Trzhaskovskaya, V.G. Yarzhemsky, Dirac-Fock photoionization parameters for HAXPES applications, Atom Data Nucl Data 119 (2018) 99-174.
[59] M.B. Trzhaskovskaya, G. Yarzhemsky, Dirac-Fock photoionization parameters for HAXPES applications, Part II: Inner atomic shells, Atom Data Nucl Data 129 (2019).
[60] M.P. Seah, A Quantitative Framework for the Analysis of Surfaces by Aes and Xps, Analusis 9(5) (1981) 171-180.
[61] S. Tanuma, C.J. Powell, D.R. Penn, Calculations of Electron Inelastic Mean Free Paths .5. Data for 14 Organic-Compounds over the 50-2000 Ev Range, Surf Interface Anal 21(3) (1994) 165-176.
[62] N. Fairley, CasaXPS, http://www.casaxps.com (2019).
[63] C.E. Ayres, B.S. Jha, H. Meredith, J.R. Bowman, G.L. Bowlin, S.C. Henderson, D.G. Simpson, Measuring fiber alignment in electrospun scaffolds: a user's guide to the 2D fast Fourier transform approach, J Biomat Sci-Polym E 19(5) (2008) 603-621.
[64] H. Alhummiany, S. Rafique, K. Sulaiman, XPS Analysis of the Improved Operational Stability of Organic Solar Cells Using a V2O5 and PEDOT:PSS Composite Layer: Effect of Varied Atmospheric Conditions, J Phys Chem C 121(14) (2017) 7649-7658.
[65] H. Yan, H. Okuzaki, Effect of solvent on PEDOT/PSS nanometer-scaled thin films: XPS and STEM/AFM studies, Synthetic Met 159(21-22) (2009) 2225-2228.
[66] K.Z. Xing, M. Fahlman, X.W. Chen, O. Inganas, W.R. Salaneck, The electronic structure of poly(3,4-ethylene-dioxythiophene): studied by XPS and UPS, Synthetic Met 89(3) (1997) 161-165.
[67] S.T. Mousavi, G.R. Harper, S. Municoy, M.D. Ashton, D. Townsend, G.H.K. Alsharif, V.K. Oikonomou, M. Firlak, S. Au-Yong, B.E. Murdock, G.R. Akien, N.R. Halcovitch, S.J. Baldock, M. Fazilati, O.V. Kolosov, B.J. Robinson, M.F. Desimone, J.G. Hardy, Electroactive Silk Fibroin Films for Electrochemically Enhanced Delivery of Drugs, Macromolecular Materials and Engineering 305(6) (2020) 2000130.
[68] M. Marzocchi, I. Gualandi, M. Calienni, I. Zironi, E. Scavetta, G. Castellani, B. Fraboni, Physical and Electrochemical Properties of PEDOT:PSS as a Tool for Controlling Cell Growth, ACS Applied Materials & Interfaces 7(32) (2015) 17993-18003.
[69] N. Casado, D. Mecerreyes, Chapter 1 Introduction to Redox Polymers: Classification, Characterization Methods and Main Applications, Redox Polymers for Energy and Nanomedicine, The Royal Society of Chemistry2021, pp. 1-26.
[70] A.V. Volkov, K. Wijeratne, E. Mitraka, U. Ail, D. Zhao, K. Tybrandt, J.W. Andreasen, M. Berggren, X. Crispin, I.V. Zozoulenko, Understanding the Capacitance of PEDOT:PSS, Advanced Functional Materials 27(28) (2017) 1700329.
[71] S.A.A. Shah, M. Firlak, S.R. Berrow, N.R. Halcovitch, S.J. Baldock, B.M. Yousafzai, R.M. Hathout, J.G. Hardy, Electrochemically Enhanced Drug Delivery Using Polypyrrole Films, Materials (Basel) 11(7) (2018).
[72] D.S. Macmillan, M.L. Chilton, A defined approach for predicting skin sensitisation hazard and potency based on the guided integration of in silico, in chemico and in vitro data using exclusion criteria, Regul Toxicol Pharmacol 101 (2019) 35-47.

[73] R.S. Foster, A. Fowkes, A. Cayley, A. Thresher, A.D. Werner, C.G. Barber, G. Kocks, R.E. Tennant, R.V. Williams, S. Kane, S.A. Stalford, The importance of expert review to clarify ambiguous situations for (Q)SAR predictions under ICH M7, Genes Environ 42 (2020) 27.
[74] A. Magaz, M.D. Ashton, R.M. Hathout, X. Li, J.G. Hardy, J.J. Blaker, Electroresponsive Silk-Based Biohybrid Composites for Electrochemically Controlled Growth Factor Delivery, Pharmaceutics 12(8) (2020).
[75] M.D. Ashton, I.C. Appen, M. Firlak, N.E. Stanhope, C.E. Schmidt, W.R. Eisenstadt, B. Hur, J.G. Hardy, Wirelessly triggered bioactive molecule delivery from degradable electroactive polymer films, Polymer International 70(4) (2021) 467-474.
[76] T. Distler, C. Polley, F. Shi, D. Schneidereit, M.D. Ashton, O. Friedrich, J.F. Kolb, J.G. Hardy, R. Detsch, H. Seitz, A.R. Boccaccini, Electrically Conductive and 3D-Printable Oxidized Alginate-Gelatin Polypyrrole:PSS Hydrogels for Tissue Engineering, Adv Healthc Mater 10(9) (2021) e2001876.
[77] K. Ohgo, C.H. Zhao, M. Kobayashi, T. Asakura, Preparation of non-woven nanofibers of Bombyx mori silk, Samia cynthia ricini silk and recombinant hybrid silk with electrospinning method, Polymer 44(3) (2003) 841-846.
[78] F. Zhang, B.Q. Zuo, Z.H. Fan, Z.G. Xie, Q. Lu, X.G. Zhang, D.L. Kaplan, Mechanisms and Control of Silk-Based Electrospinning, Biomacromolecules 13(3) (2012) 798-804.
[79] A. Ajisawa, Dissolution of silk fibroin with calciumchloride/ethanol aqueous solution, The Journal of Sericultural Science of Japan 67(2) (1998) 91-94.
[80] S.H. Kim, Y.S. Nam, T.S. Lee, W.H. Park, Silk fibroin nanofiber. Electrospinning, properties, and structure, Polym J 35(2) (2003) 185-190.
[81] S. Sukigara, M. Gandhi, J. Ayutsede, M. Micklus, F. Ko, Regeneration of Bombyx mori silk by electrospinning - part 1: processing parameters and geometric properties, Polymer 44(19) (2003) 5721-5727.
[82] B.M. Min, G. Lee, S.H. Kim, Y.S. Nam, T.S. Lee, W.H. Park, Electrospinning of silk fibroin nanofibers and its effect on the adhesion and spreading of normal human keratinocytes and fibroblasts in vitro, Biomaterials 25(7-8) (2004) 1289-1297.
[83] K.H. Zhang, Q.Z. Yu, X.M. Mo, Fabrication and Intermolecular Interactions of Silk Fibroin/Hydroxybutyl Chitosan Blended Nanofibers, Int J Mol Sci 12(4) (2011) 2187-2199.
[84] J.P. Chen, S.H. Chen, G.J. Lai, Preparation and characterization of biomimetic silk fibroin/chitosan composite nanofibers by electrospinning for osteoblasts culture, Nanoscale Res Lett 7 (2012) 1-11.
[85] Z. Liu, F. Zhang, J.F. Ming, S.Y. Bie, J.J. Li, B.Q. Zuo, Preparation of Electrospun Silk Fibroin Nanofibers from Solutions Containing Native Silk Fibrils, J Appl Polym Sci 132(1) (2015).
[86] C.L. Mo, P.Y. Wu, X. Chen, Z.Z. Shao, The effect of water on the conformation transition of Bombyx mori silk fibroin, Vib Spectrosc 51(1) (2009) 105-109.
[87] H. Okuzaki, S. Takagi, F. Hishiki, R. Tanigawa, Ionic liquid/polyurethane/PEDOT:PSS composites for electro-active polymer actuators, Sensors and Actuators B: Chemical 194 (2014) 59-63.
[88] L. Laflamme, M. Gasparo, J.M. Gallo, M.D. Payet, N. Gallo-Payet, Angiotensin II induction of neurite outgrowth by AT2 receptors in NG108-15 cells. Effect counteracted by the AT1 receptors, J Biol Chem 271(37) (1996) 22729-35.
[89] J.G. Hardy, H. Li, J.K. Chow, S.A. Geissler, A.B. McElroy, L. Nguy, D.S. Hernandez, C.E. Schmidt, Conducting polymer-based multilayer films for instructive biomaterial coatings, Future Science OA 1(4) (2015).
[90] Y. Qiu, R. Liao, X. Zhang, Impedance-based monitoring of ongoing cardiomyocyte death induced by tumor necrosis factor-alpha, Biophys J 96(5) (2009) 1985-91.
[91] M.K.U. Sikder, W. Tong, H. Pingle, P. Kingshott, K. Needham, M.N. Shivdasani, J.B. Fallon, P. Seligman, M.R. Ibbotson, S. Prawer, D.J. Garrett, Laminin coated diamond electrodes for neural stimulation, Mater Sci Eng C Mater Biol Appl 118 (2021) 111454.